Własności transportowe niejednorodnych nanodrutów półprzewodnikowych

Maciej Wołoszyn

współpraca:
Janusz Adamowski
Bartłomiej Spisak
Paweł Wójcik

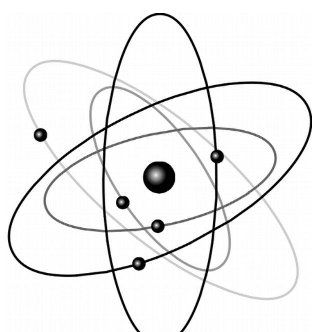

Seminarium WFiIS AGH
13 stycznia 2017

Streszczenie

- nanodruty półprzewodnikowe zawierające warstwy różnych materiałów → struktury tunelowo-rezonansowe
- układy kwaziperiodyczne w nanodrutach
- nanodruty o niejednorodnej geometrii → przewężenia, pole magnetyczne i ich wpływ na transport ładunku i spinu elektronów

Badania były finansowane przez Narodowe Centrum Nauki w ramach grantu DEC-2011/03/B/ST3/00240.

[1] M.Wołoszyn, B.J.Spisak, P.Wójcik, J.Adamowski, Physica E 83 (2016) 12
[2] M.Wołoszyn, B.J.Spisak, J.Adamowski, P.Wójcik, J. Phys.: Condens. Matter 26 (2014) 325301
[3] M.Wołoszyn, J.Adamowski, P.Wójcik and B.J.Spisak, J. Appl. Phys. 114 (2013) 164301
[4] B.J. Spisak , M.Wołoszyn, D.Szydłowski, J. Comput. Electron. 14 (2015) 916
[5] D.Szydłowski, M.Wołoszyn, B.J.Spisak, Semicond. Sci. Technol. 28 (2013) 105022
[6] M.Wołoszyn, B.J.Spisak, Eur. Phys. J. B 85 (2012) 10
[7] B.J.Spisak, M.Wołoszyn, Phys. Rev. B 80 (2009) 035127

Nanodruty

- struktury o średnicach rzędu kilku-kilkunastu nanometrów
- stosunek długość/promień (*aspect ratio*) typowo rzędu 100-1000
- inaczej druty kwantowe z powodu zasadniczego znaczenia zjawisk kwantowych

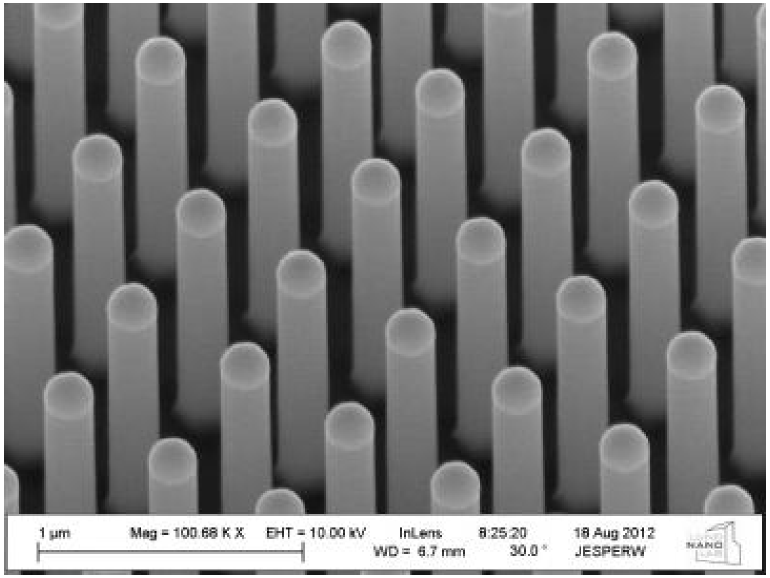

- przykładowe zastosowania:
  - nanoelektronika i spintronika (np.. tranzystory, sensory, filtry spinowe)
  - fotonika i fotowoltaika (LED, ogniwa)
  - technologie pozwalające na magazynowanie energii

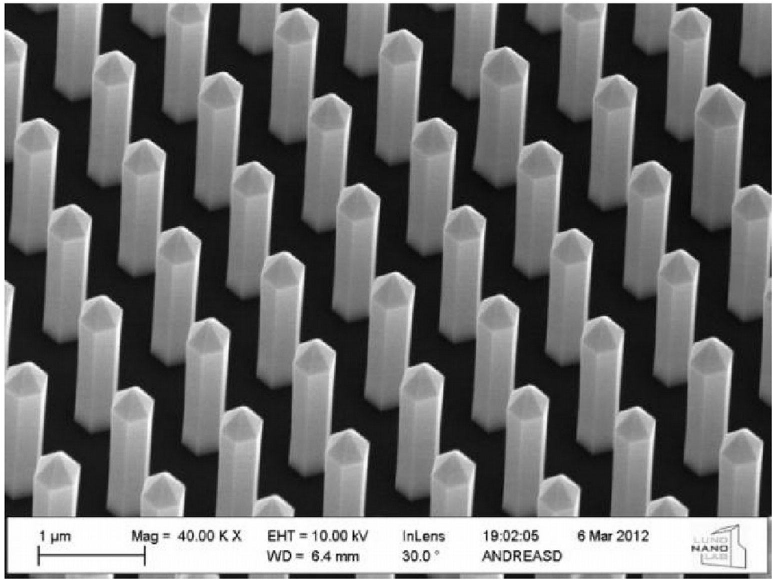

Tunelowanie rezonansowe przez układ dwóch barier w nanodrucie InAs/InP

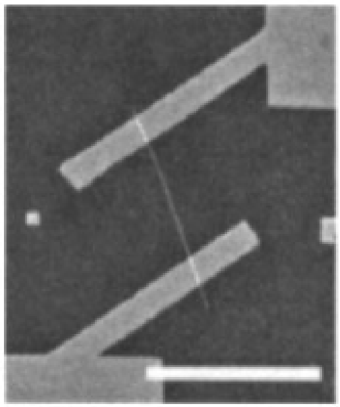

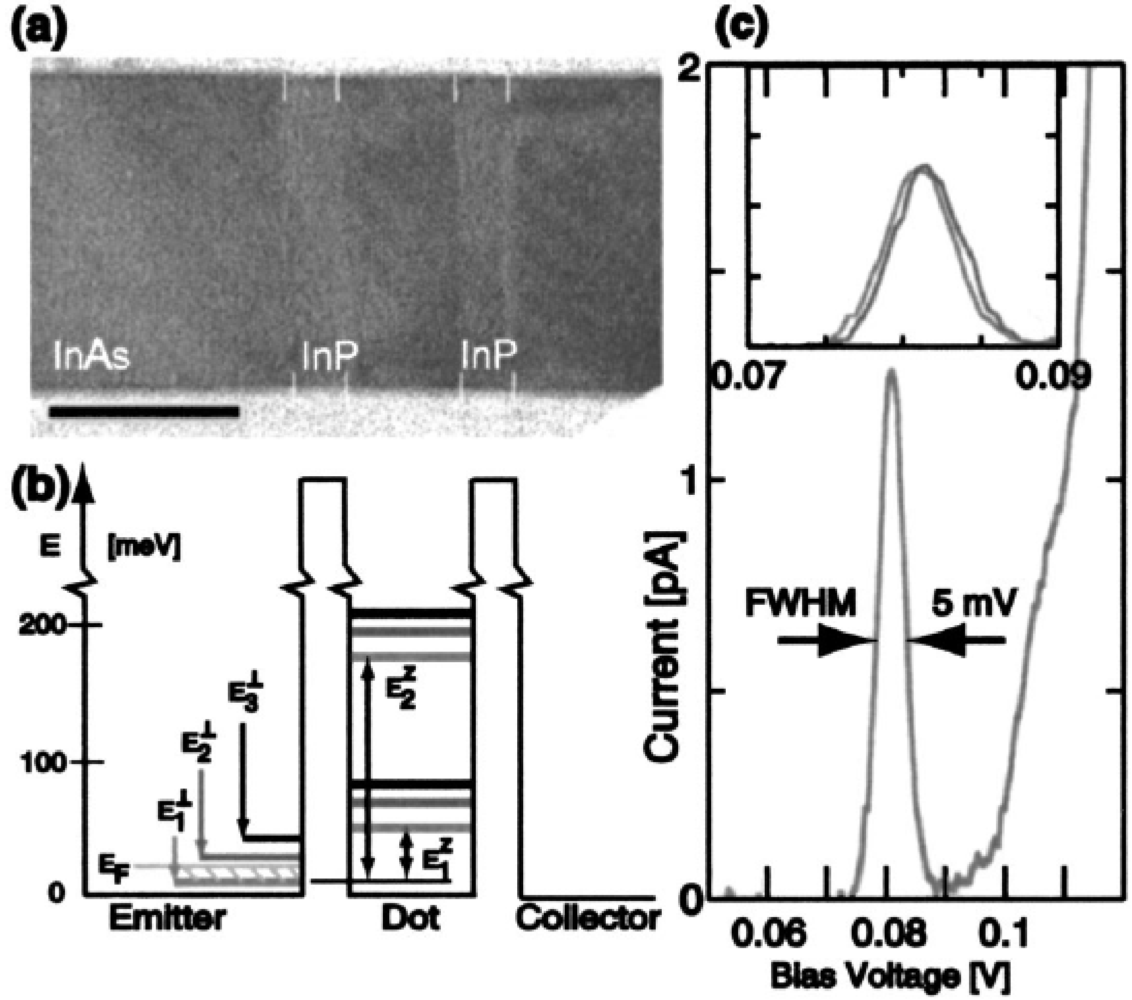

[Björk et.al. Appl Phys Lett **81,** 4458 (2002)]

Przybliżenie adiabatyczne

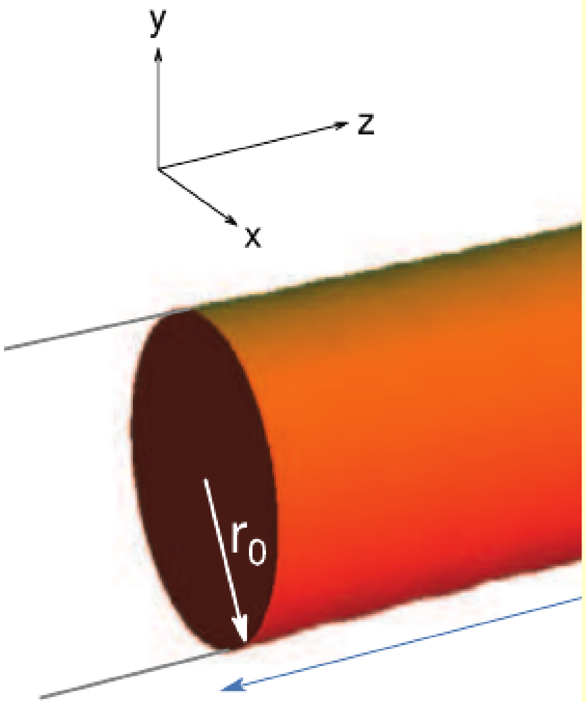

$$\hat{\mathcal{H}} = \frac{\hat{\mathbf{p}}^2}{2m^*} + U_{\mathrm{conf}}(\mathbf{r})$$

$$\psi(x, y, z) = \sum_s \phi_s(z)\chi_s(x, y; z)$$

$$U(z) = U_{db}(z) + U_F(z)$$

$$U_F(z) = \begin{cases} 0 & \text{for} \quad z \leq 0, \\ eFz & \text{for} \quad 0 \leq z \leq L, \\ -eV & \text{for} \quad z \geq L. \end{cases}$$

$$U_{db}(z) = U_b\left[\mathrm{e}^{-\left(\frac{z-z_1}{R}\right)^p} + \mathrm{e}^{-\left(\frac{z-z_2}{R}\right)^p}\right]$$

Przybliżenie adiabatyczne

$$\hat{\mathcal{H}} = \frac{\hat{\mathbf{p}}^2}{2m^*} + U_{\mathrm{conf}}(\mathbf{r}) \qquad \& \qquad \psi(x,y,z) = \sum_s \phi_s(z)\chi_s(x,y;z)$$

$$\chi_s(x,y;z) = \sum_{k=1}^{N_x}\sum_{l=1}^{N_y} c_{kl}^s(z)\, g_{kl}(x,y;z)$$

$$g_{kl}(x,y;z) = \exp\left[-\frac{(x-x_k)^2+(y-y_l)^2}{2\sigma^2}\right]$$

$$E_s^{\perp}(z) \qquad \chi_s(x,y;z)$$

$$\left[-\frac{\hbar^2}{2m^*}\frac{d^2}{dz^2} + E_s^{\perp}(z) - E\right]\phi_s(z) = \sum_{s'}\left[\hat{\mathcal{T}}_{ss'}(z) + \hat{\mathcal{A}}_{ss'}(z)\right]\phi_{s'}(z)$$

$$\hat{\mathcal{T}}_{ss'}(z) = \int dxdy\; \chi_s^*(x,y;z)\frac{\hat{p}_z^2}{2m^*}\chi_{s'}(x,y;z)$$

$$\hat{\mathcal{A}}_{ss'}(z) = \int dxdy\; \chi_s^*(x,y;z)\frac{\hat{p}_z}{m^*}\chi_{s'}(x,y;z)\hat{p}_z$$

(jeśli można zaniedbać)

$$\left[-\frac{\hbar^2}{2m^*}\frac{d^2}{dz^2} + E_s^{\perp}(z)\right]\phi_s(z) = E\phi_s(z)$$

QTBM

$$T_s(E)$$

Oscylacje prądowe na skutek rezonansów Starka

$$I(V) = \frac{2e}{h} \int_{-\infty}^{\infty} T(E,V)[f_S(E) - f_D(E)]\mathrm{d}E$$

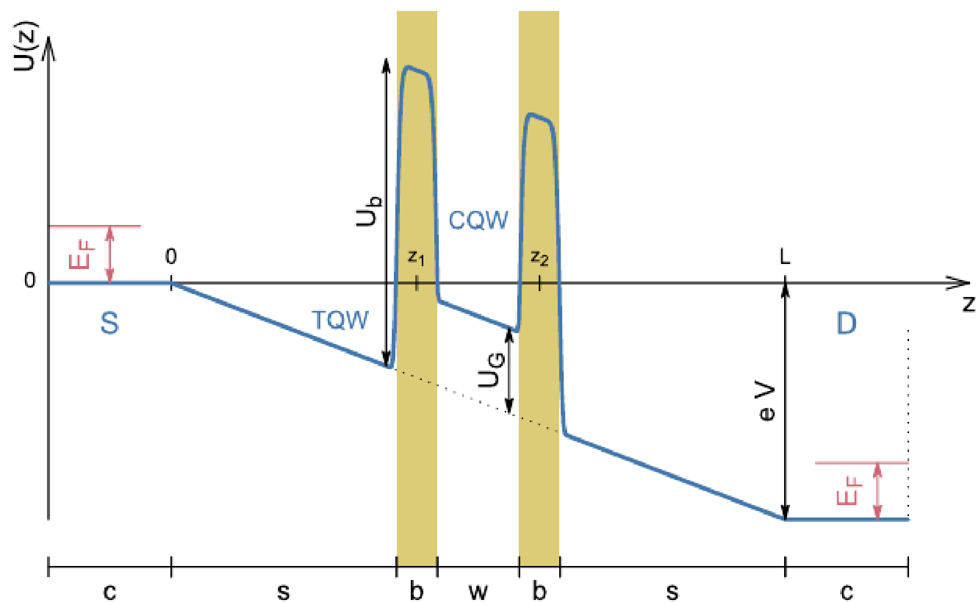

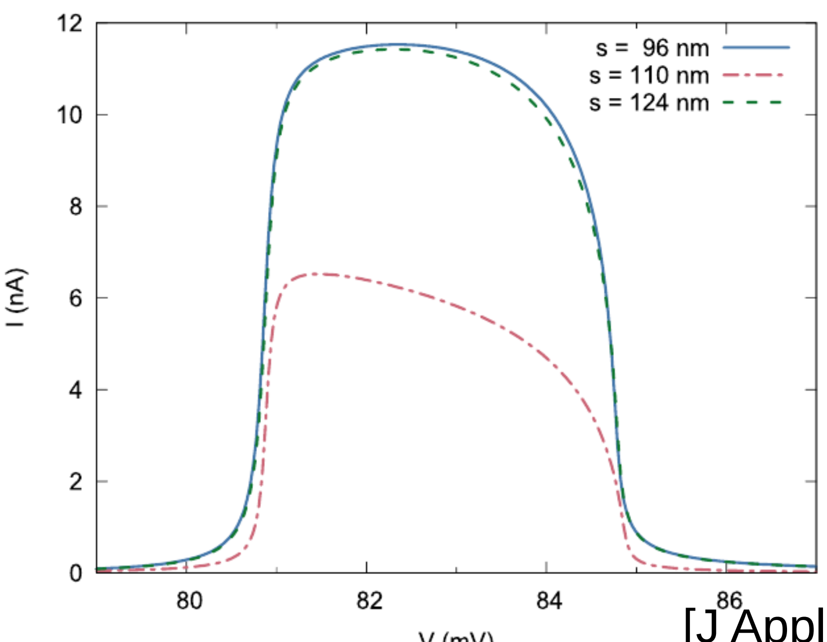

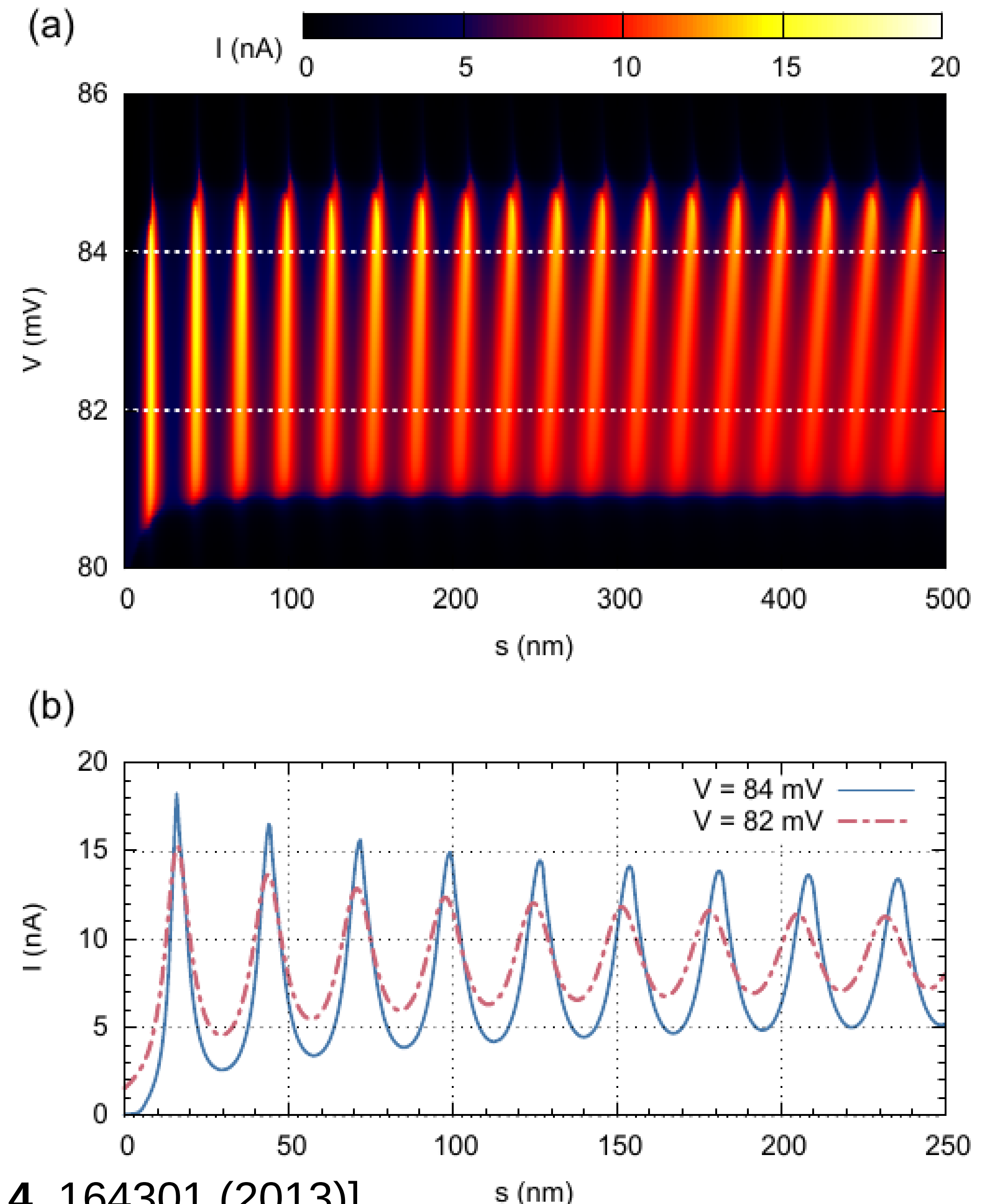

[J Appl Phys **114**, 164301 (2013)]

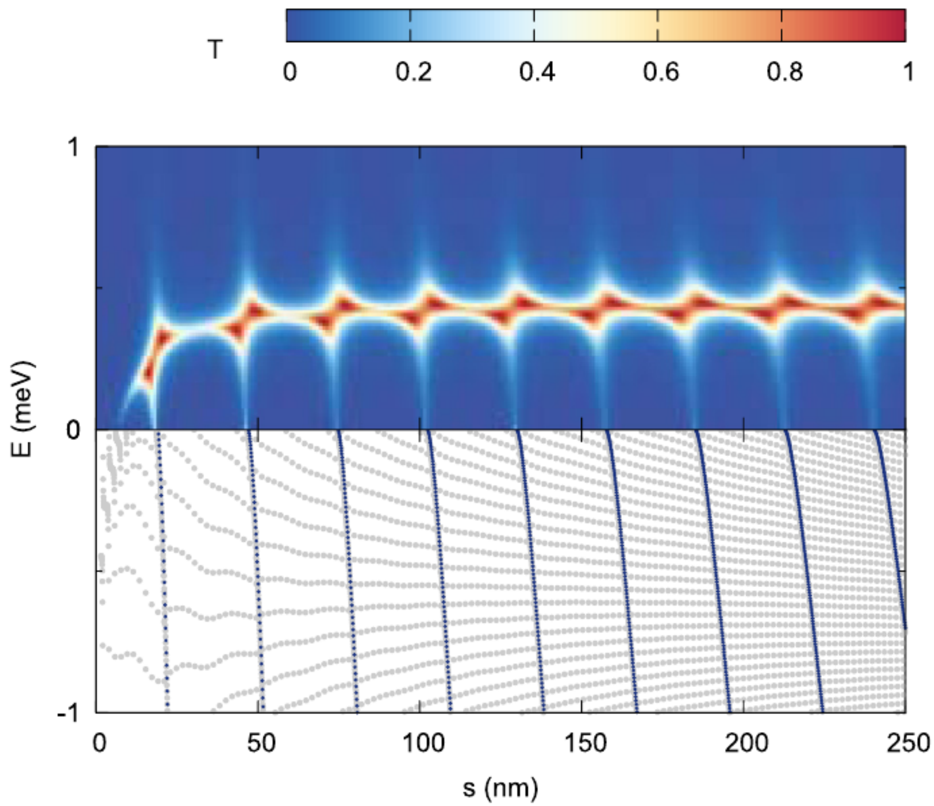

FIG. 6. Upper part: Transmission coefficient T as a function of energy E and spacer width s. Lower part: energy levels E_n of the quasi-bound states as functions of the spacer width s. Gray dots show the energies calculated for the entire nanodevice (including the contacts) and blue dots show the energy levels of the quasi-bound states localized in the left spacer. The calculations have been performed for $V = 84\,\mathrm{mV}$ and $U_G = 0$.

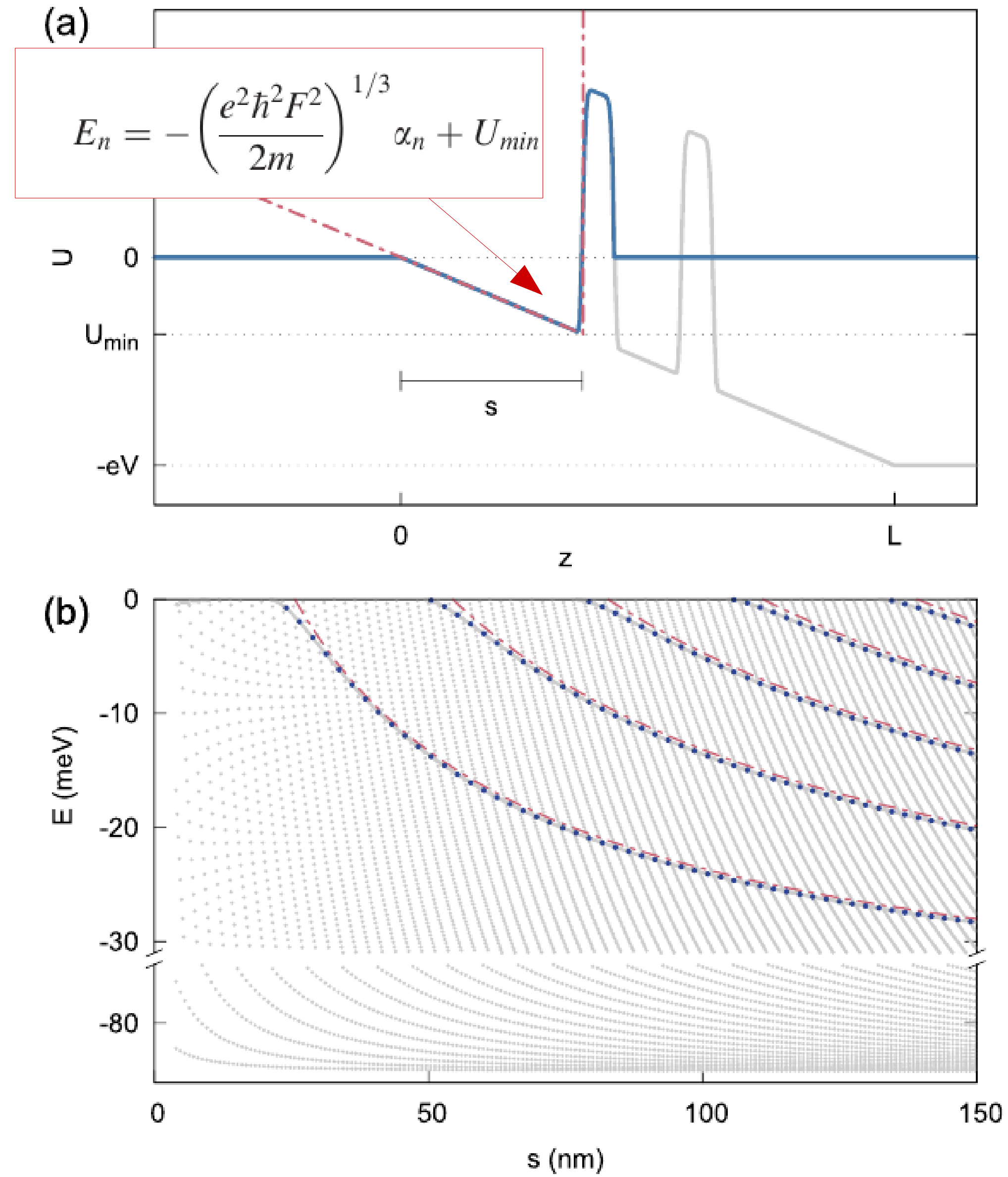

FIG. 8. (a) Potential energy profiles for the entire nanosystem (gray lines), the simple model with the left spacer and barrier (blue lines), and the infinite TQW (red dash-doted lines) corresponding to the profile of the triangular potential well in the left spacer region. The widths of the different regions and the barrier heights are not to scale, $U_{min} = -eVs/L$. (b) Energy eigenvalues calculated for the potential energy profiles plotted in panel (a) as functions of the spacer width s for $V = 84\,\mathrm{mV}$ and $U_G = 0$. The symbols and colors of the curves correspond to those in panel (a).

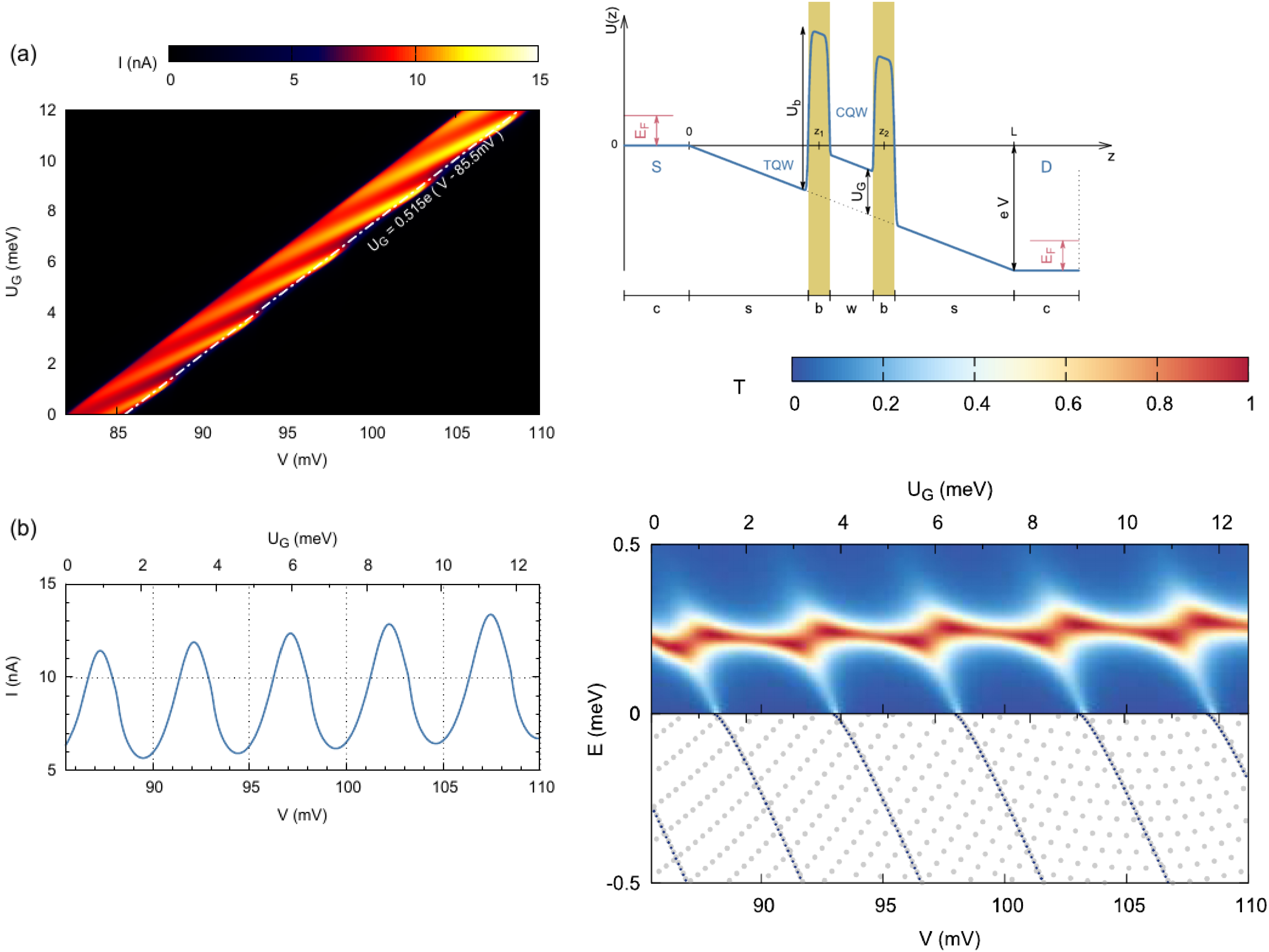
(a)
I (nA)
0
5
10
15
U_G (meV)
V (mV)
$U_G = 0.515e\,(V - 85.5\mathrm{mV})$
U(z)
U_b
CQW
E_F
0
z_1
z_2
L
z
S
TQW
U_G
D
e V
E_F
c
s
b
w
b
s
c
T
0
0.2
0.4
0.6
0.8
1
(b)
U_G (meV)
I (nA)
V (mV)
U_G (meV)
E (meV)
V (mV)

Nanodruty z wieloma barierami

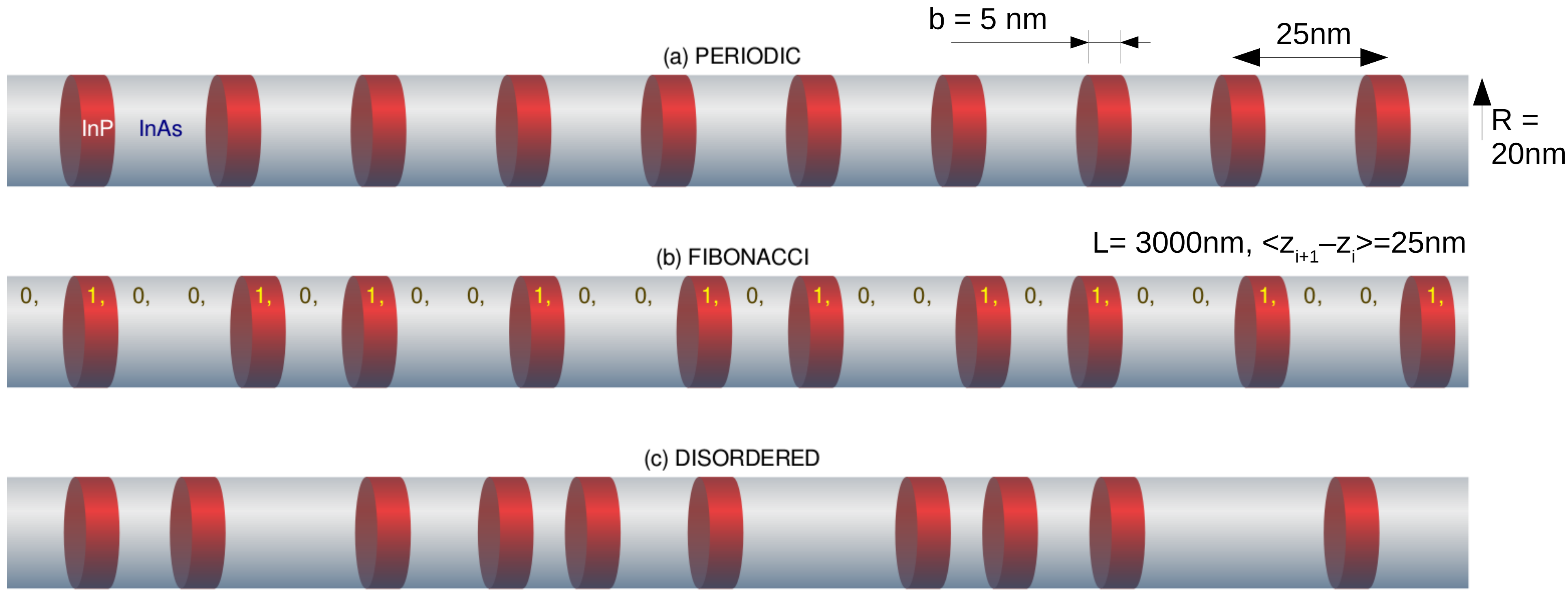

$$U_{\rm conf}(x,y,z) = U_\perp(x,y;z) + U_\parallel(z)$$

$$U_\perp(x,y;z) = \begin{cases} 0 & \text{for } x^2+y^2 \le R \\ U_0 & \text{for } x^2+y^2 > R \end{cases} \qquad U_\parallel(z) = U_B \sum_{i=1}^{N_B} \exp\left[-\left(\frac{z-z_i}{b/2}\right)^p\right]$$

$$U_0 = 2 \text{ eV.} \qquad U_B = 0.6 \text{ eV}, \; p=6 \quad N_B = 100.$$

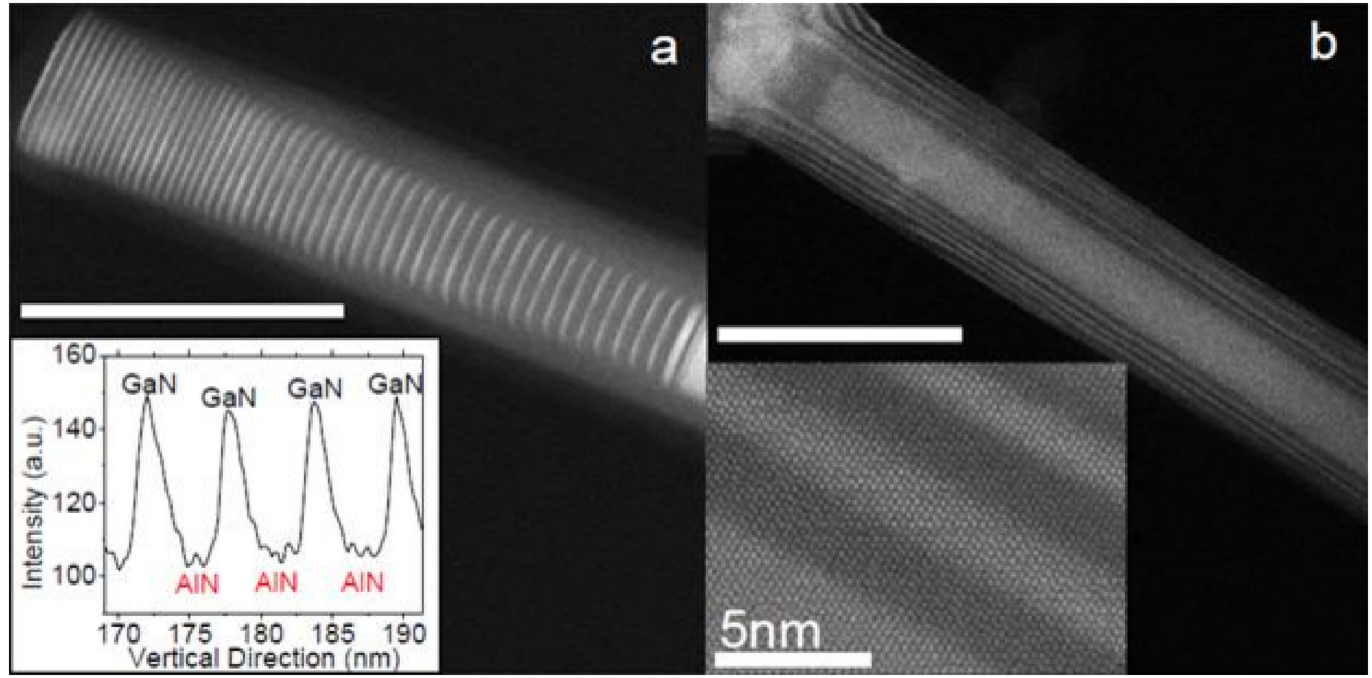

(a) 50 period vertically-aligned AlN/GaN nanowire superlattice prepared using the two-step method. Bottom Inset: profile intensity scan measuring compositional modulation along the vertical c-axis direction. (b) 5 period coaxially-aligned AlN/GaN nanowire superlattice using the two-step procedure. Bottom Inset: section of coaxial layers imaged with atomic resolution. Dark (light) areas correspond to AlN (GaN) due to z-contrast. All scale bars correspond to 100 nm unless labeled otherwise.

[Carnevale et al., Nano Lett. **11**, 866 (2011)]

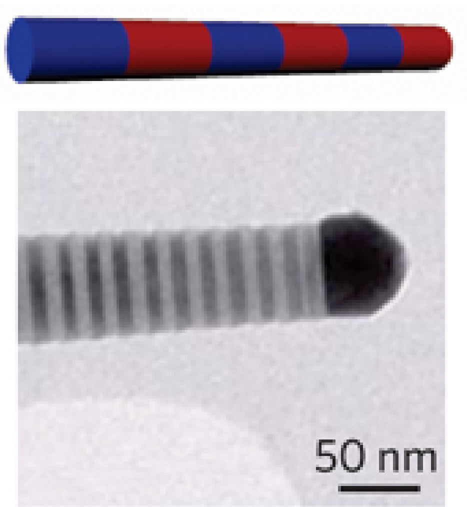

Schematic (top) and TEM image of an InP superlattice nanowire.

[Yan et al., Nature Photonics **3**, 569 (2009)]

Układy kwaziperiodyczne

- tradycyjna klasyfikacja materii (w dużym uproszczeniu):
  - materiały krystaliczne (uporządkowanie)
  - materiały amorficzne (nieporządek)

- w kręgu zainteresowań matematyków, fizyków teoretyków również m. in. :
  - ciągi aperiodyczne
  - aperiodyczne pokrycia płaszczyzny (np. *Parkietaż Penrose'a*)

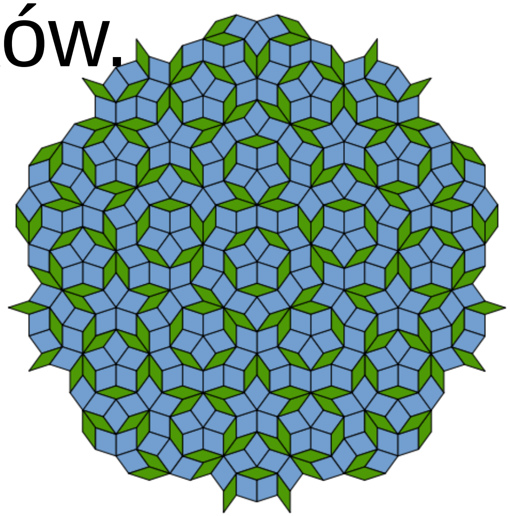

Kwazikryształy

- Dan Shechtman, 1984

  Stop Al-Mn dający obraz dyfrakcyjny jak dla kryształów, ale z 5-krotną osią symetrii

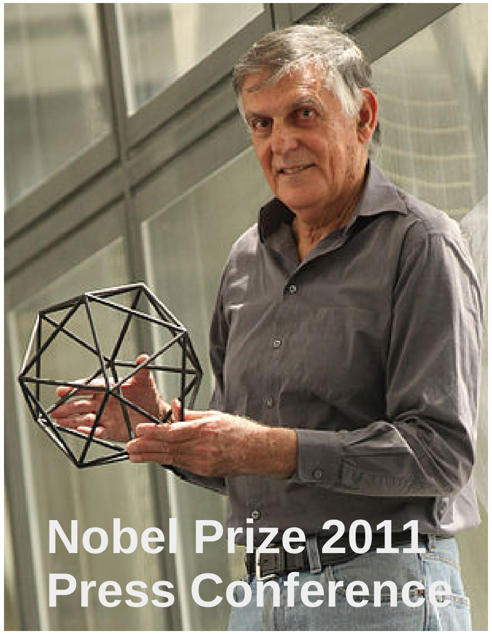

Pierwszy znaleziony naturalnie występujący kwazikryształ (prawdopodobnie z meteorytu):

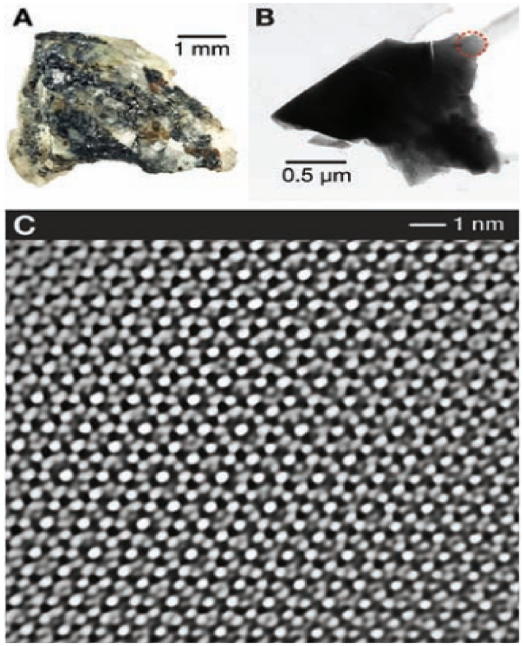

Fig. 1. (**A**) The original khatyrkite-bearing sample used in the study. The lighter-colored material on the exterior contains a mixture of spinel, augite, and olivine. The dark material consists predominantly of khatyrkite ($CuAl_2$) and cupalite (CuAl) but also includes granules, like the one in (**B**), with composition $Al_{63}Cu_{24}Fe_{13}$. The diffraction patterns in Fig. 4 were obtained from the thin region of this granule indicated by the red dashed circle, an area 0.1 μm across. (**C**) The inverted Fourier transform of the HRTEM image taken from a subregion about 15 nm across displays a homogeneous, quasiperiodically ordered, fivefold symmetric, real space pattern characteristic of quasicrystals.

[Bindi et.al. Science ***324,*** *1306 (2009)]*

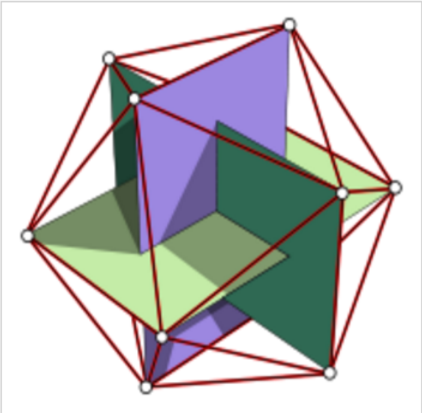

Icosahedron vertices form three orthogonal golden rectangles [wikipedia]

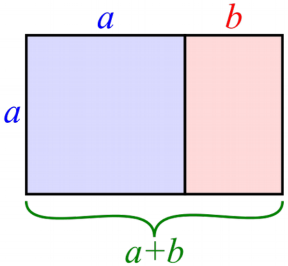

$$\frac{a+b}{a} = \frac{a}{b} \stackrel{\text{def}}{=} \varphi,$$

$$\varphi = \frac{1+\sqrt{5}}{2} = 1.6180339887\ldots.$$

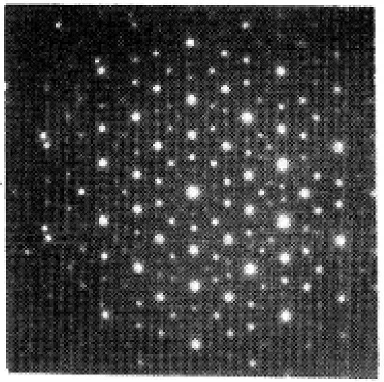

Diffraction pattern taken from a single grain of the icosahedral phase.

- opór właściwy różnych typów materiałów (w temperaturze pokojowej)

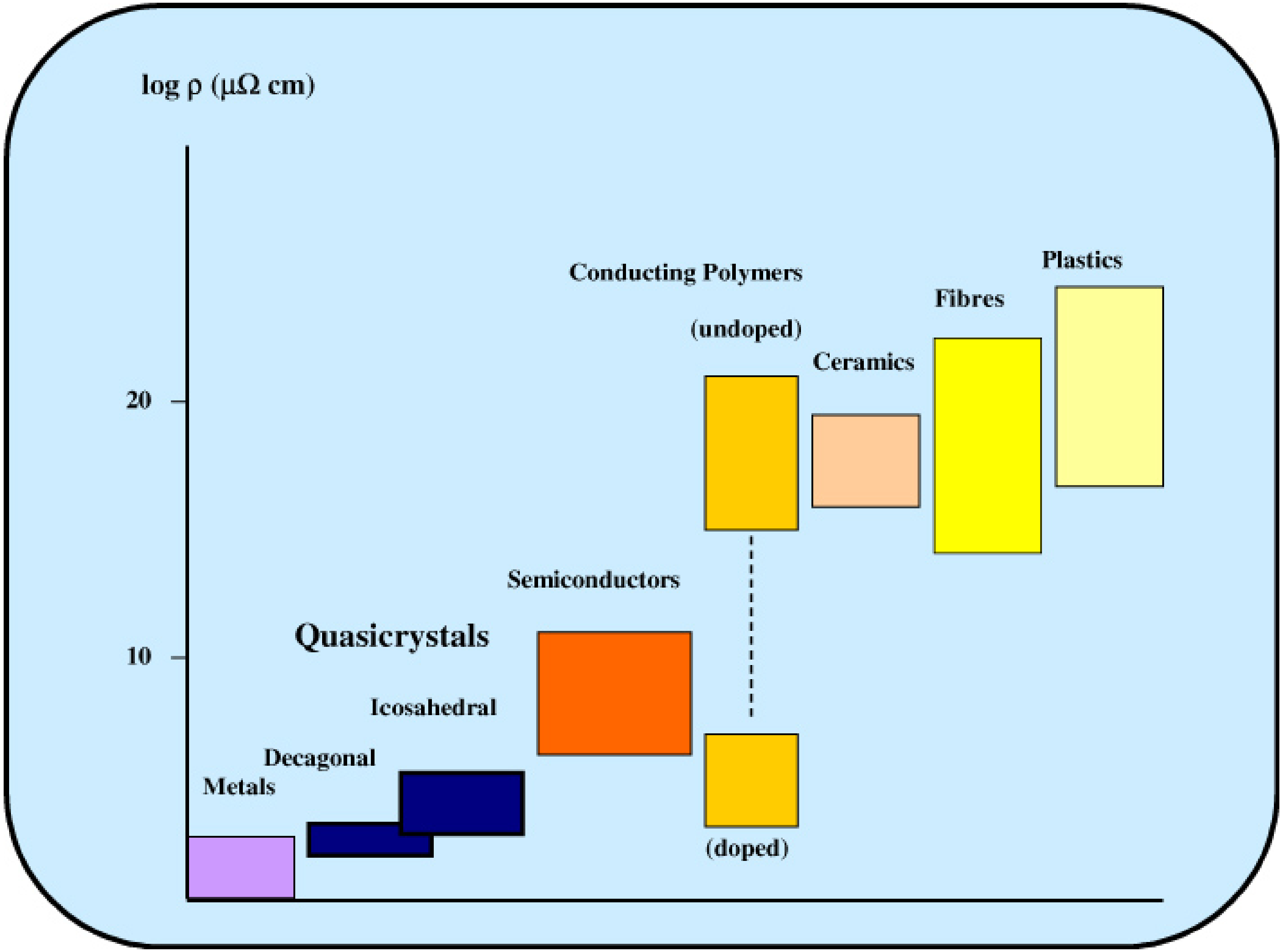

*[E.Maciá, Rep Prog Phys **69,** 397 (2006)]*

Reguły podstawień generujące ciągi o własnościach aperiodycznych i samopodobnych

Sequence	Set L	Substitution rule
Fibonacci	$\{A, B\}$	$g(A) = AB \; g(B) = A$
Thue–Morse	$\{A, B\}$	$g(A) = AB \; g(B) = BA$
Period-doubling	$\{A, B\}$	$g(A) = AB \; g(B) = AA$
Silver mean	$\{A, B\}$	$g(A) = AAB \; g(B) = A$
Bronze mean	$\{A, B\}$	$g(A) = AAAB \; g(B) = A$
Copper mean	$\{A, B\}$	$g(A) = ABB \; g(B) = A$
Nickel mean	$\{A, B\}$	$g(A) = ABBB \; g(B) = A$
Triadic Cantor	$\{A, B\}$	$g(A) = ABA \; g(B) = BBB$
Rudin–Shapiro	$\{A, B, C, D\}$	$g(A) = AC \; g(B) = DC \; g(C) = AB \; g(D) = DB$
Paper folding	$\{A, B, C, D\}$	$g(A) = AB \; g(B) = CB \; g(C) = AD g(D) = CD$

[*E.Maciá, Rep Prog Phys* ***69,*** *397 (2006)*]

Binarny ciąg Fibonacciego
(*"Fibonacci word"*)

- generowany przez:
  {0} → {0,1}
  {1} → {0}

n-ty wyraz: $f(n) = 2+\lfloor n\varphi \rfloor - \lfloor (n+1)\varphi \rfloor$

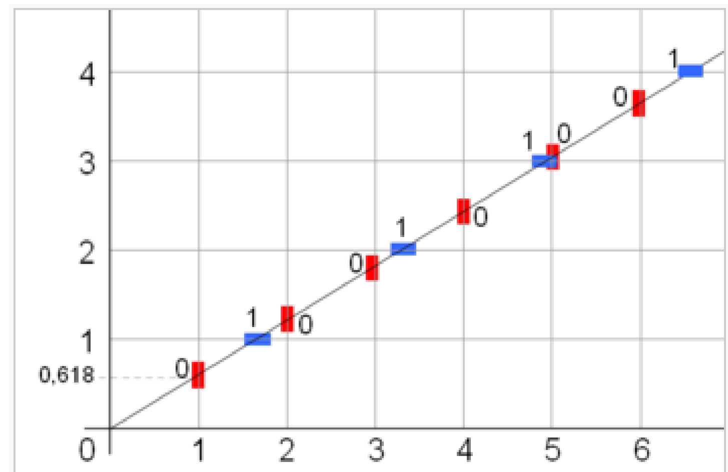

Characterization by a cutting sequence with a line of slope $1/\varphi$ or $\varphi - 1$, with φ the golden ratio.

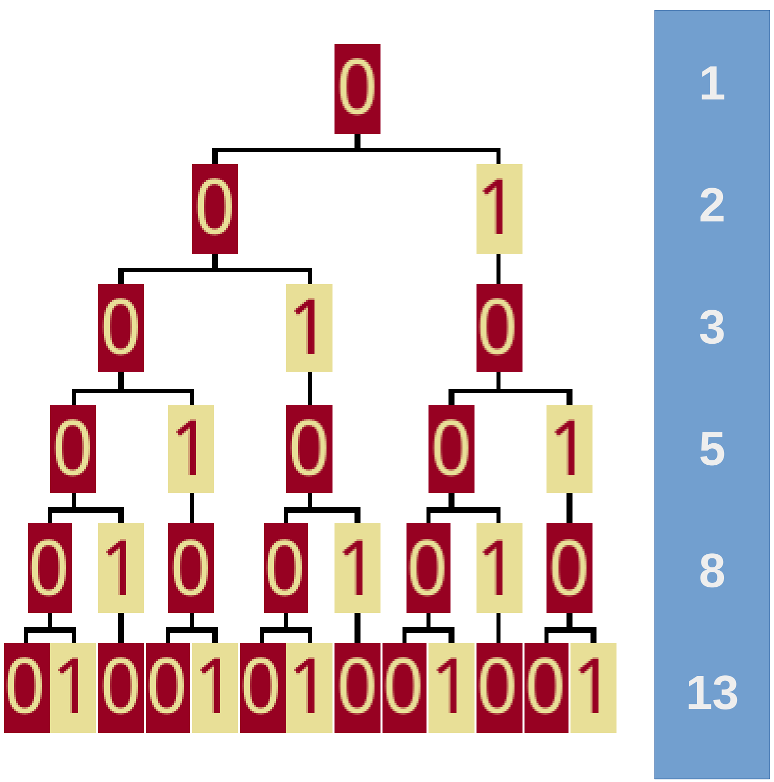

długość = liczba Fibonacciego F(n)

$$F(n) = F(n-1) + F(n-2)$$

$$\lim_{n\to\infty} F(n+1)/F(n) = \varphi$$

Fibonacci word i fraktale

- konstrukcja fraktala

dla każdego *f(n)* :

- narysuj jednostkowy odcinek
- jeśli *f(n)=0* wykonaj zwrot o 90°:
    - w prawo jeśli *n* jest parzyste
    - w lewo jeśli *n* jest nieparzyste

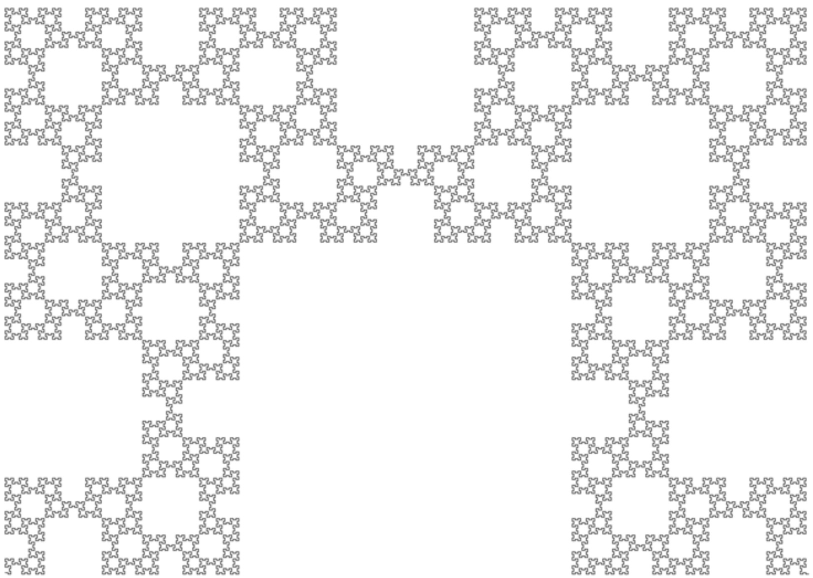

wymiar fraktalny Hausdorffa:

3 log(φ)/log(1+√2) ≈ 1.638

- rozpraszanie elektronów w 1-wymiarowym układzie opartym na binarnym ciągu Fibonacciego

Nomata et al. PHYSICAL REVIEW B **76**, 235113 (2007)

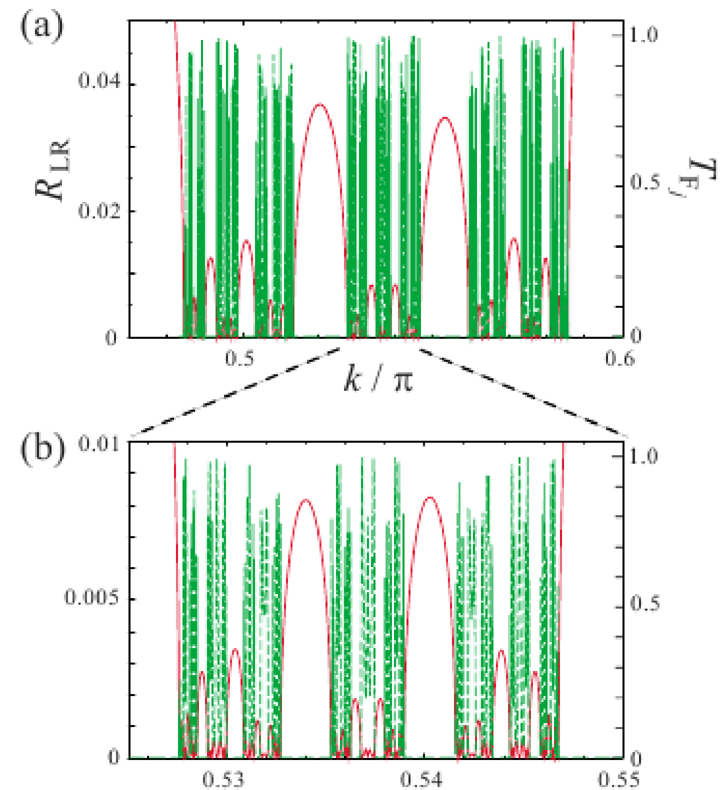

FIG. 7. (Color online) Self-similarity for transmission probability and Landauer resistance at $j=17$, $\ell=L_A=1$, and $L_B=0.5$. The green dashed line is T_{F_j} and the red solid line is R_{LR}. (a) depicts the region $0.47 \leqslant k/\pi \leqslant 0.60$ and (b) shows the enlarged region of $0.47 \leqslant k/\pi \leqslant 0.60$.

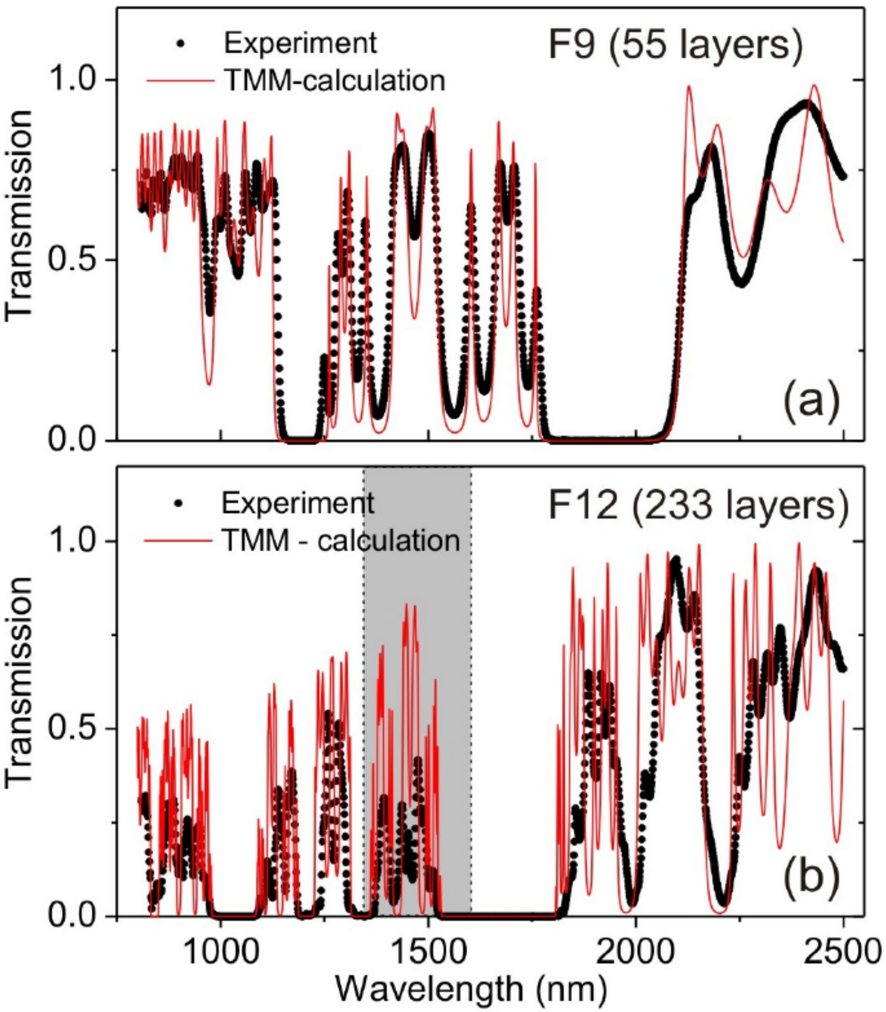

FIG. 8. (a) The transmission spectrum of the porous silicon-based F9 sample is compared to the transfer-matrix calculations with 1% of optical path gradient. (b) The same for the F12 sample. The gradient is of 4% in this case.

[Ghulinyan et al., Phys Rev B **71**, 094204 (2005)]

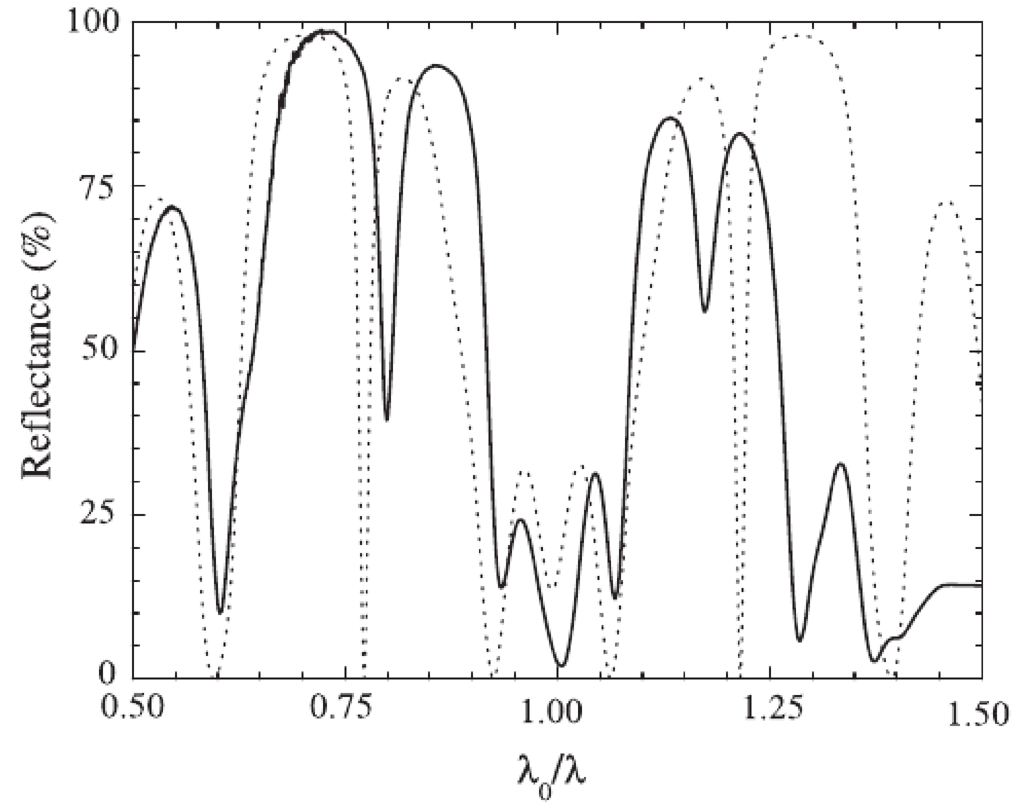

Figure 4. Experimental (solid line) and theoretical (dashed line) reflectance spectra of the asymmetric Fibonacci array S_6 made of porous silicon, where $\lambda_0 = 600$ nm.

[Nava et al., J Phys Cond Mat **21**, 155901 (2009)]

Binarny ciąg Thue-Morse'a (*"Thue-Morse word"*)

- generowany przez:

  {0} → {0,1}

  {1} → {1,0}

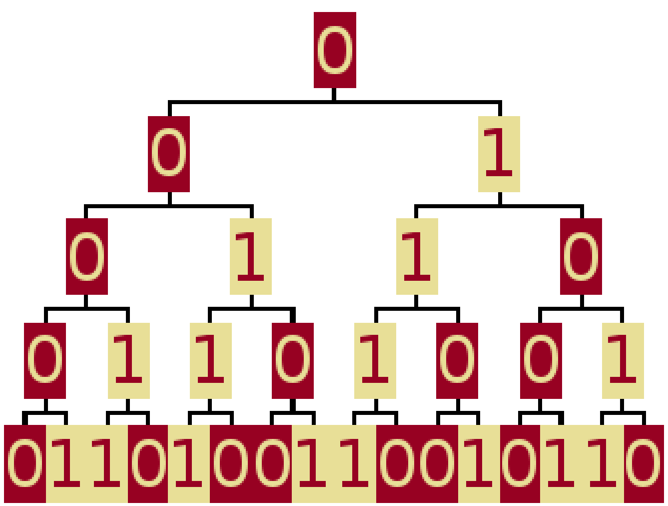

- konstrukcja fraktala

  dla każdego *t(n)* :

  - jeśli *t(n)=0* : narysuj odcinek jednostkowy

  - jeśli *t(n)=1* : wykonaj zwrot o 60° (*przeciwnie do ruchu wskazówek zegara*)

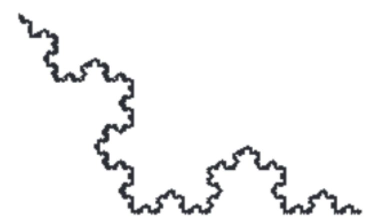

FIGURE 3. The Thue-Morse turtle program of degree 14

wymiar fraktalny Hausdorffa:

$\ln 4 / \ln 3 \approx 1.262$

Konduktancja

$$G(E) = \frac{2e^2}{h} \sum_s T_s(E)$$

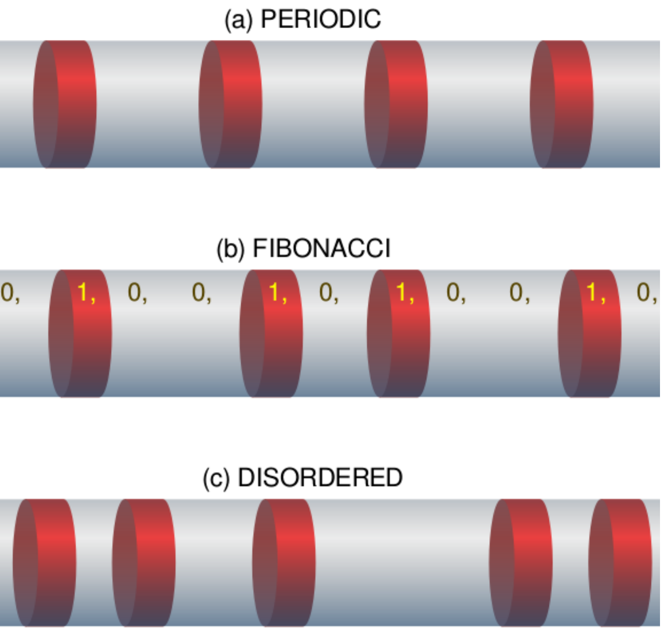

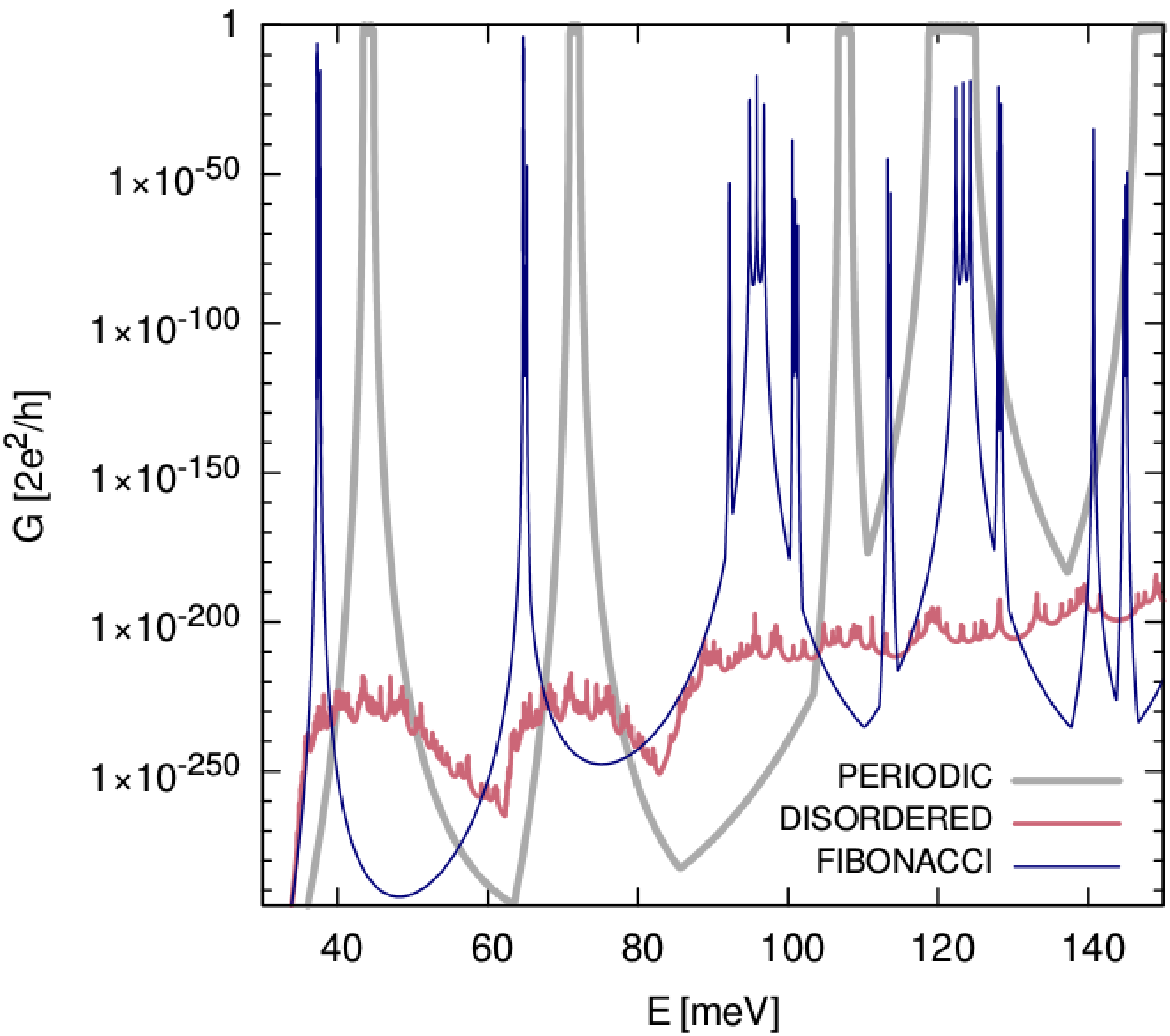

Współczynnik transmisji

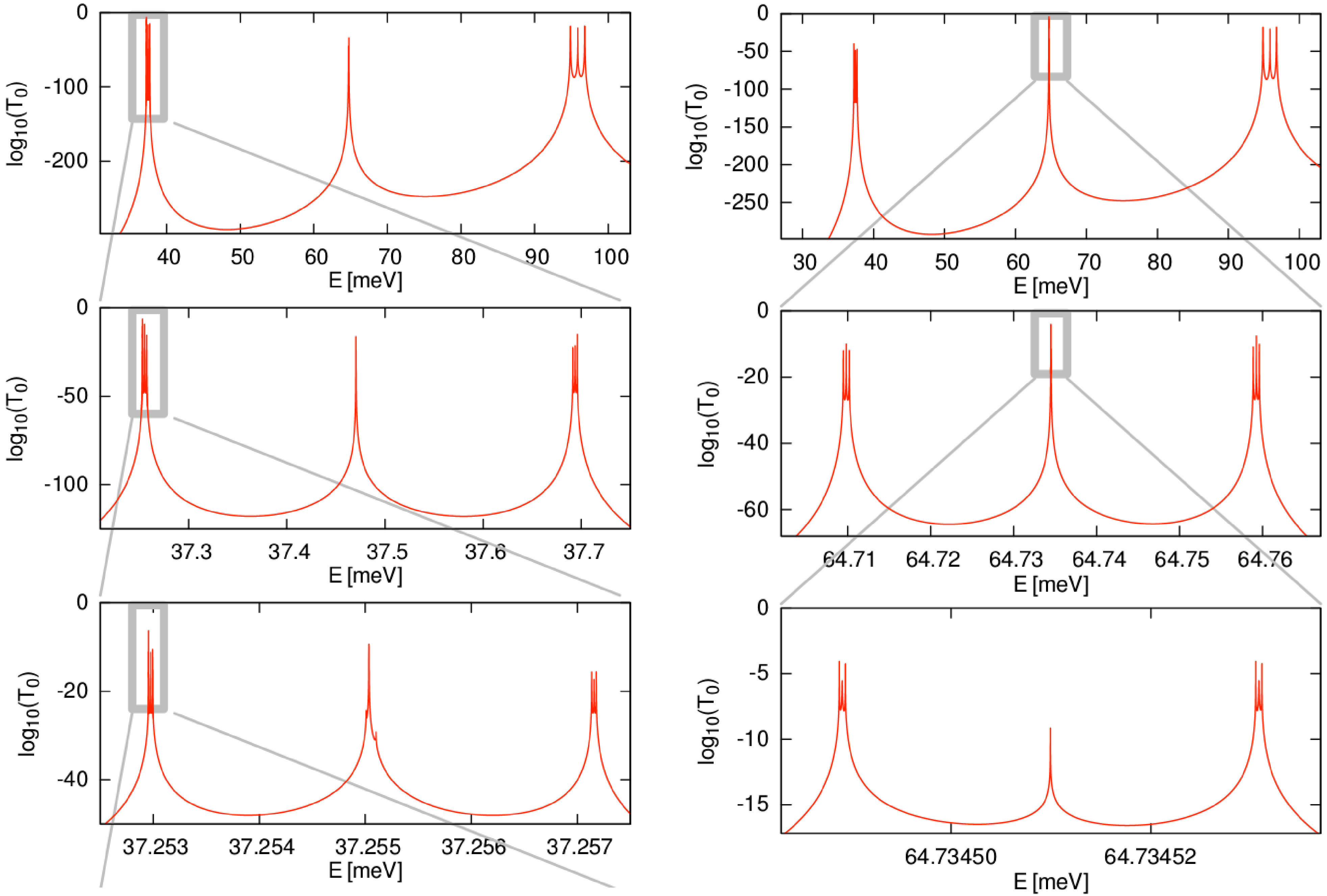

Opis za pomocą funkcji Wignera

$$\frac{\partial \rho_W(x,p,t)}{\partial t} + \frac{p}{m^*}\frac{\partial \rho_W(x,p,t)}{\partial x} = \frac{1}{2\pi\hbar}\int dp'\, \mathcal{U}_W(x,p-p')\rho_W(x,p',t),$$

$$\mathcal{U}_W(x,k-k') = \int dx' \left[U\left(x+\frac{x'}{2}\right) - U\left(x-\frac{x'}{2}\right) \right] e^{-(i/\hbar)(p-p')x'}$$

$$U(x) = U_0 \sum_k \exp\left[-\left(\frac{x-x_k}{w}\right)^2 \right] \qquad x_k^P = ka$$

$$U_0 = 2, \quad w = 0.25 \qquad \overline{(x^F_{k+1} - x^F_k)} = \overline{(x^{TM}_{k+1} - x^{TM}_k)} = \overline{(x^D_{k+1} - x^D_k)} = a = 6$$

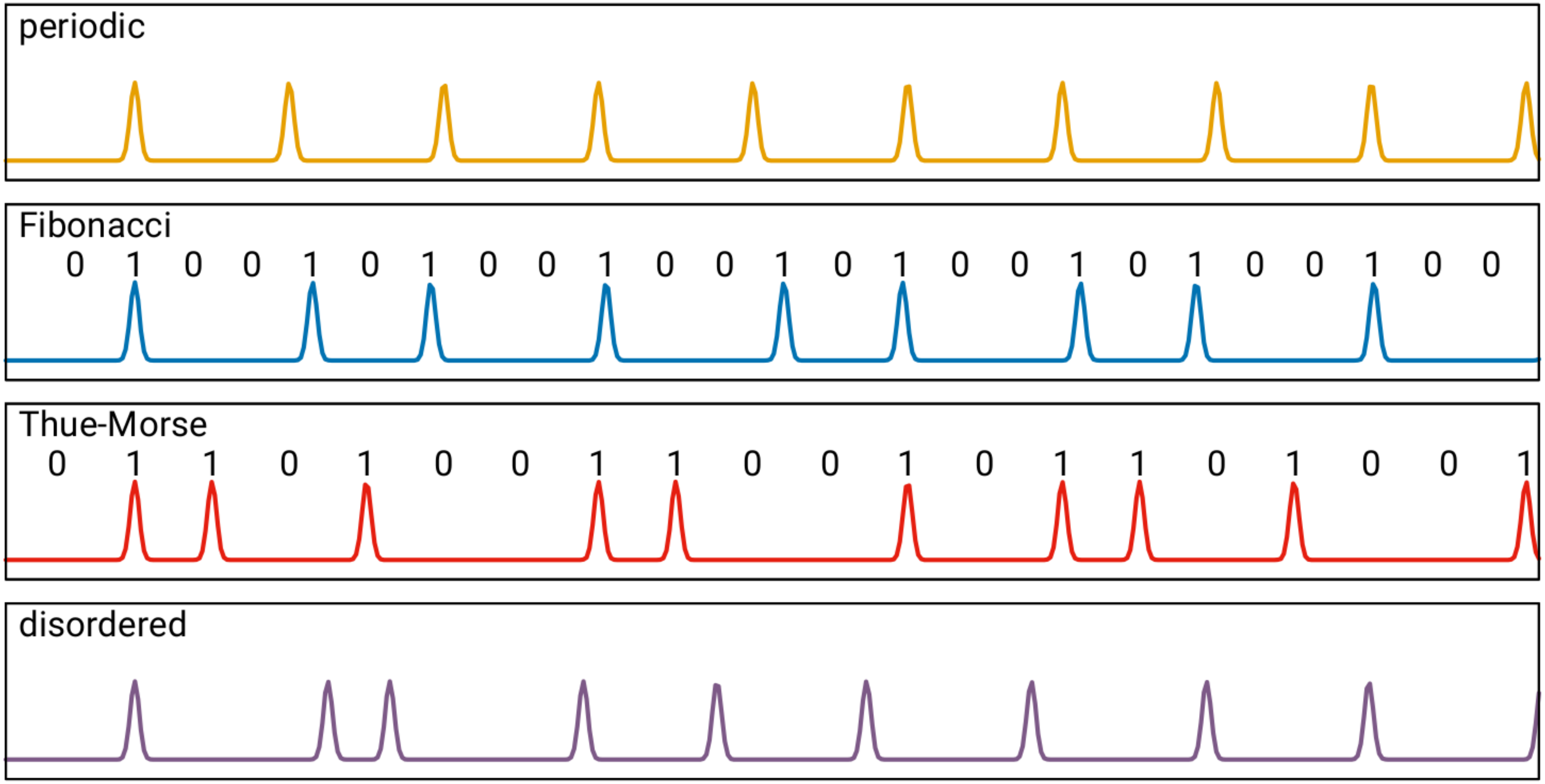

Funkcja Wignera – ewolucja czasowa

jednostki atomowe $(e = \hbar = m_e = 1)$

$$\rho_W(x, p, t=0) = \frac{1}{\pi} \exp\left[-\frac{(x-x_0)^2}{2\delta_x^2} - \frac{(p-p_0)^2}{2\delta_p^2} \right]$$

$$\delta_x = \frac{\sqrt{2}}{2}\ , \quad \delta_p = \frac{\hbar}{2\delta_x} = \frac{\sqrt{2}}{2}\ , \quad x_0 = 0\ , \quad p_0 = 2$$

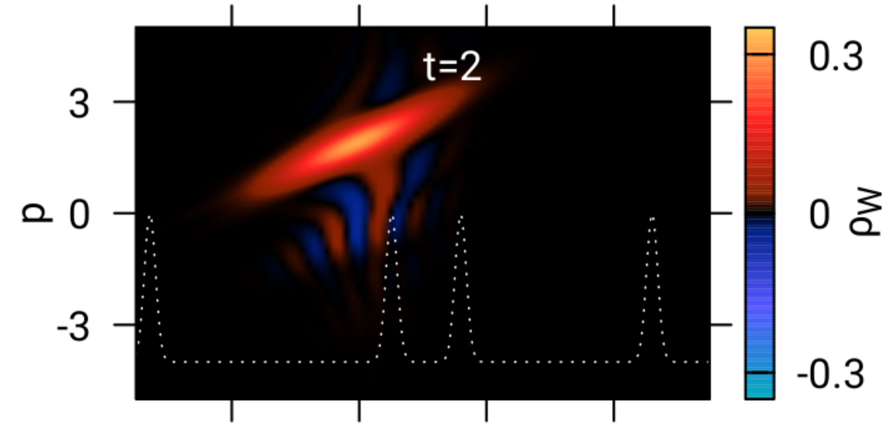

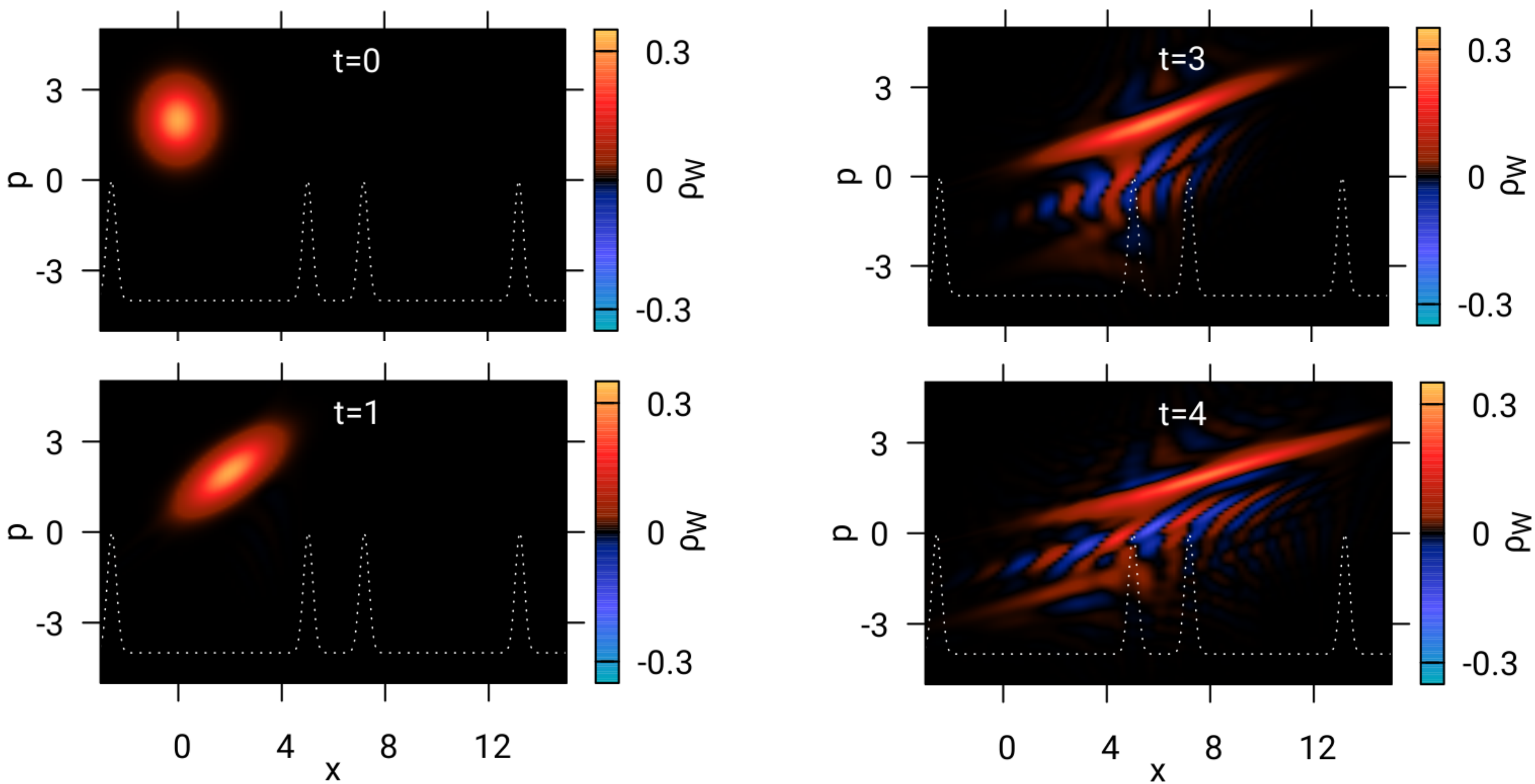

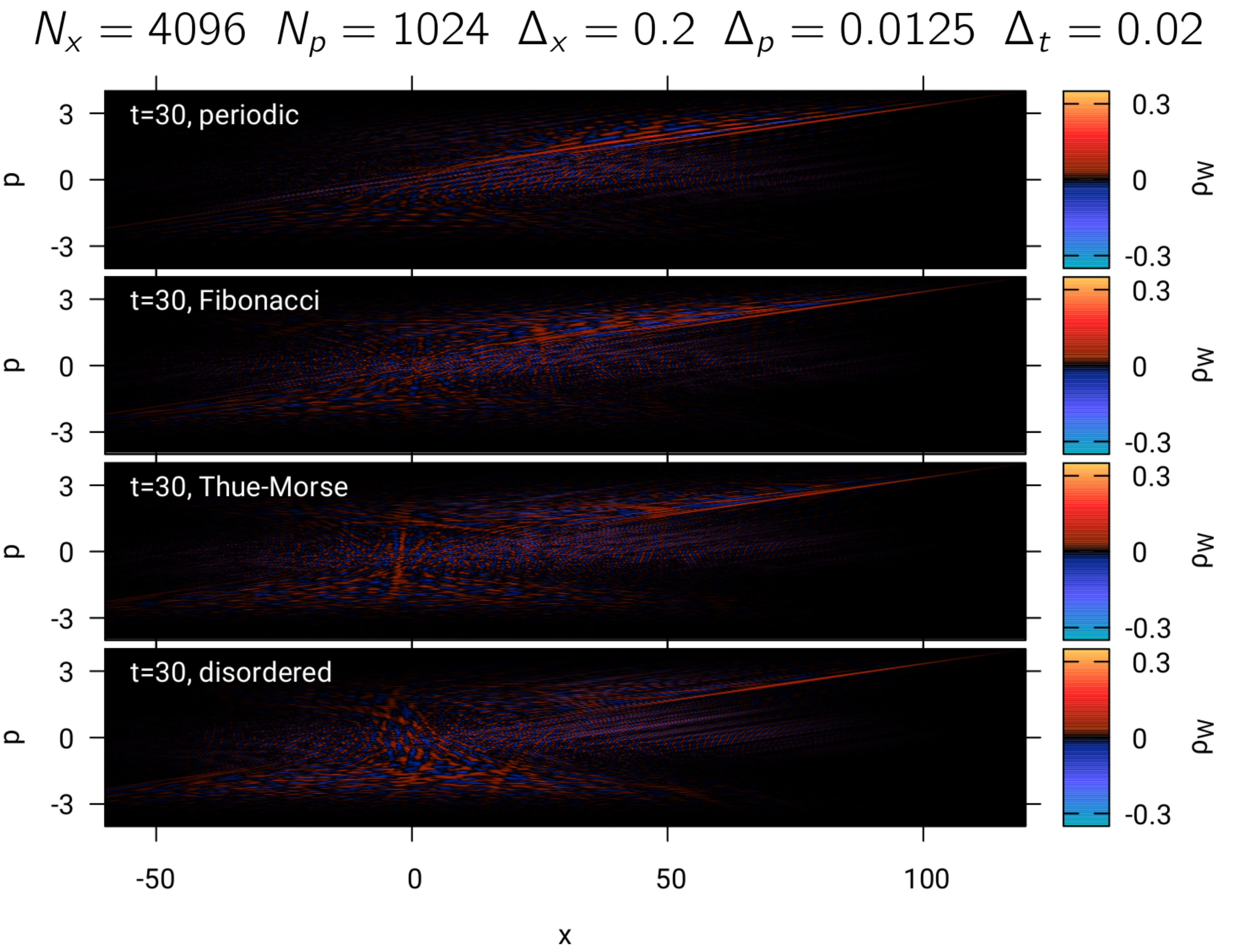

$N_x = 4096$ $N_p = 1024$ $\Delta_x = 0.2$ $\Delta_p = 0.0125$ $\Delta_t = 0.02$
t=30, periodic
t=30, Fibonacci
t=30, Thue-Morse
t=30, disordered
p
x
ρ_W
3
0
-3
-50
0
50
100
0.3
0
-0.3

$$\langle x(t)\rangle = \frac{1}{2\pi\hbar}\int x\,\rho_W(x,p,t)\,\mathrm{d}x\mathrm{d}p$$

$$\langle p(t)\rangle = \frac{1}{2\pi\hbar}\int p\,\rho_W(x,p,t)\,\mathrm{d}x\mathrm{d}p$$

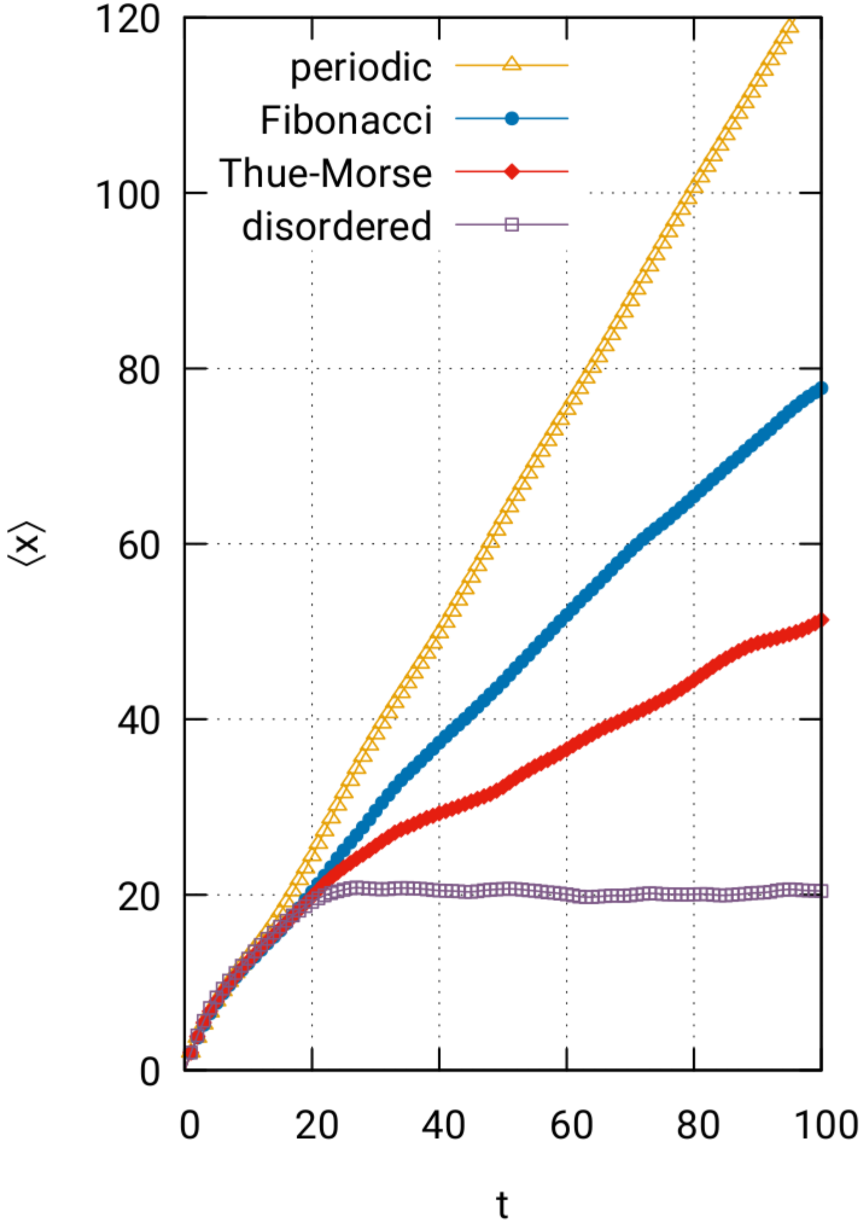

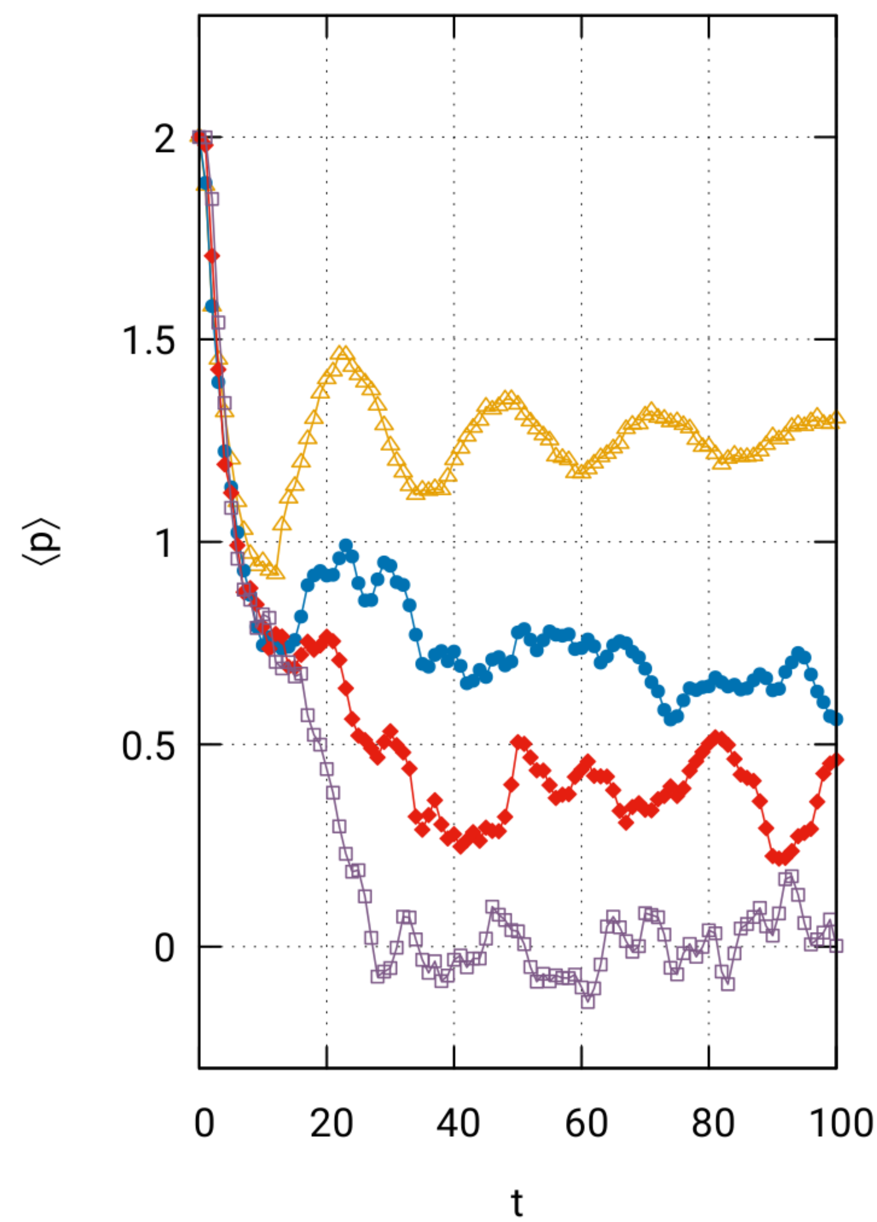

Trajektorie
w przestrzeni fazowej (<x>, <p>)

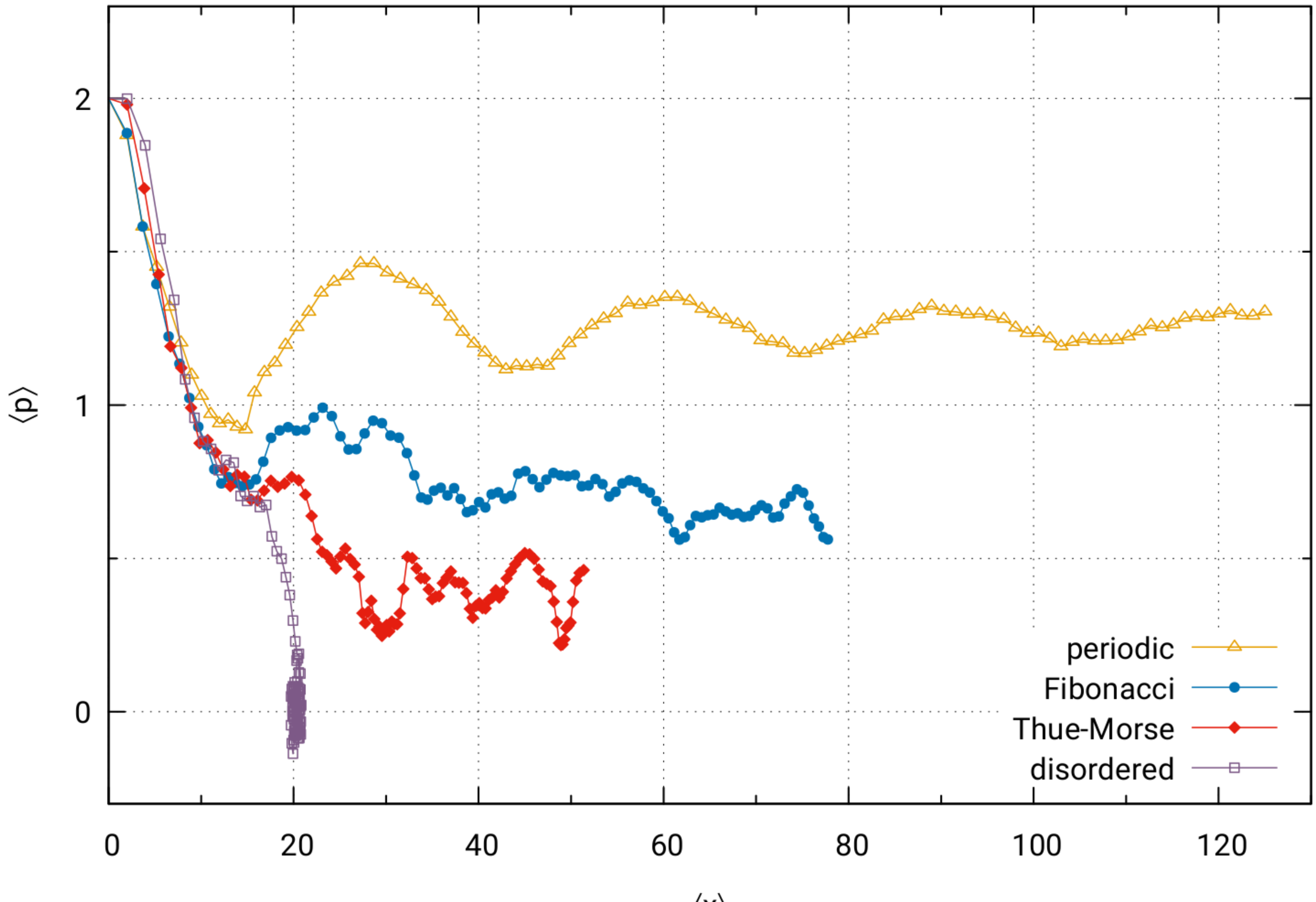

Parametr nieklasyczności

$$\rho_W(x,p,t) = \rho_W^+(x,p,t) + \rho_W^-(x,p,t)$$

$$\mathcal{I}_n^{\pm} = \left| \int dx dk \, \rho_W^{\pm}(x,p,t) \right|$$

$$\nu = 1 - \frac{\mathcal{I}^+ - \mathcal{I}^-}{\mathcal{I}^+ + \mathcal{I}^-}$$

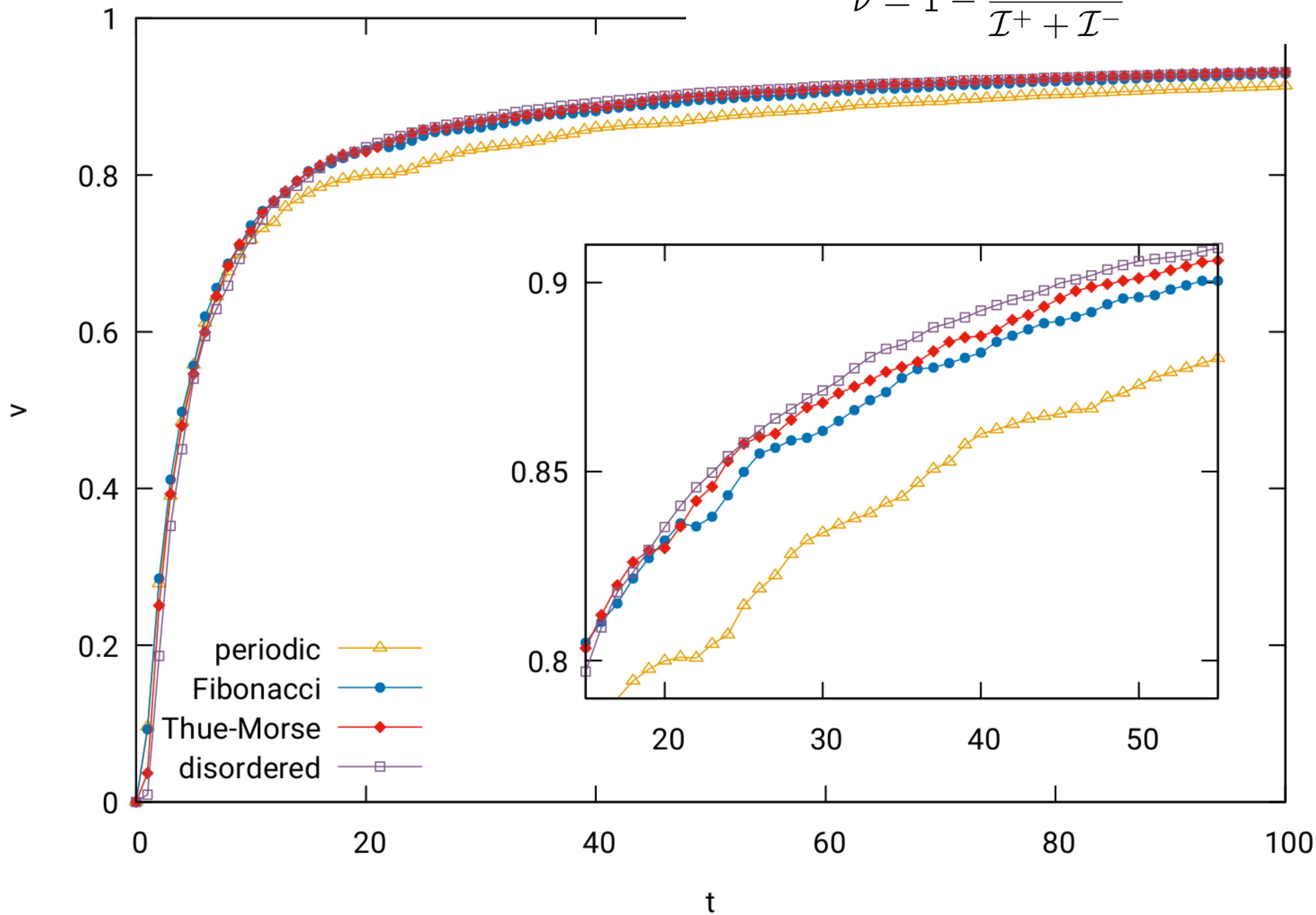

$$\langle x^2(t)\rangle = \frac{1}{2\pi\hbar}\int x^2 \rho_W(x,p,t)\,\mathrm{d}x\mathrm{d}p \quad \propto \quad t^{\alpha}$$

- α = 1 → dyfuzja
- 1 < α < 2 → transport superdyfuzyjny
- α = 2 → transport balistyczny

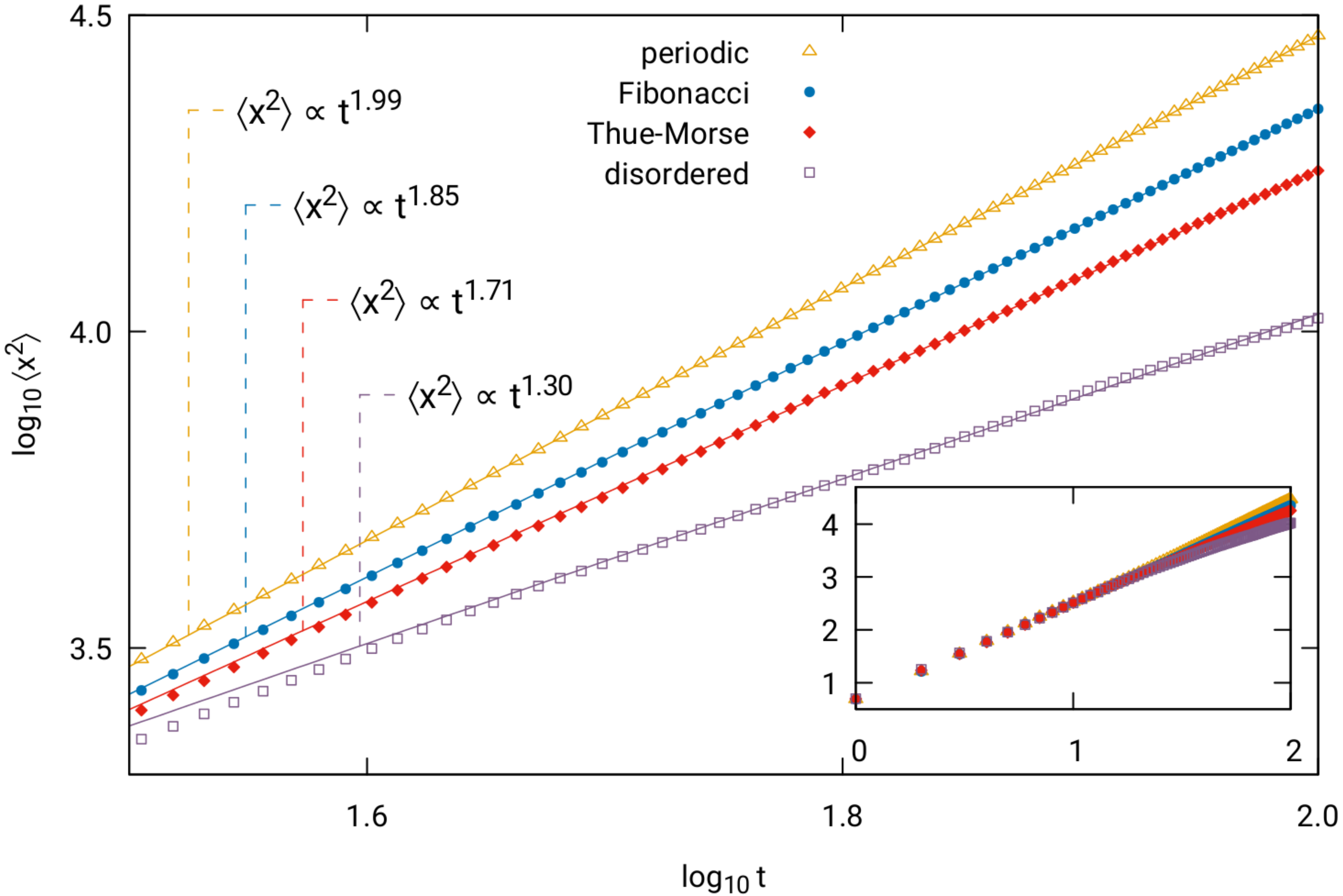

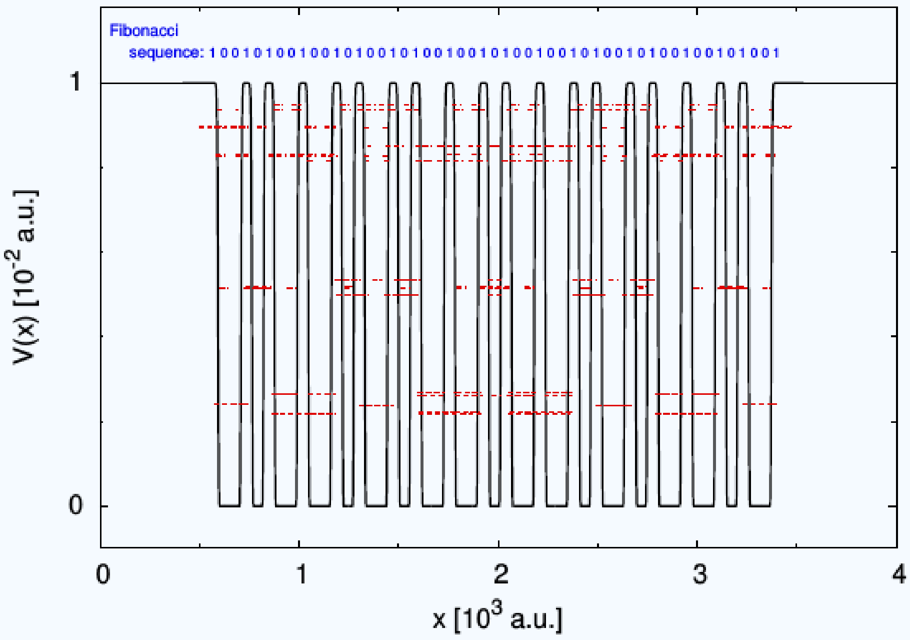

Figure 1. Potential energy profile of the Fibonacci superlattice formed by 20 layers of $Al_{0.3}Ga_{0.7}As$ and 31 layers of GaAs for when no external electric field is applied. The electronic states are plotted as (red) horizontal lines at their energies, with lines plotted for those x at which $|\psi_n^2(x)|$ exceeds its average value.

$$\mathrm{IPR} = \int dx\, |\psi_n(x)|^4$$

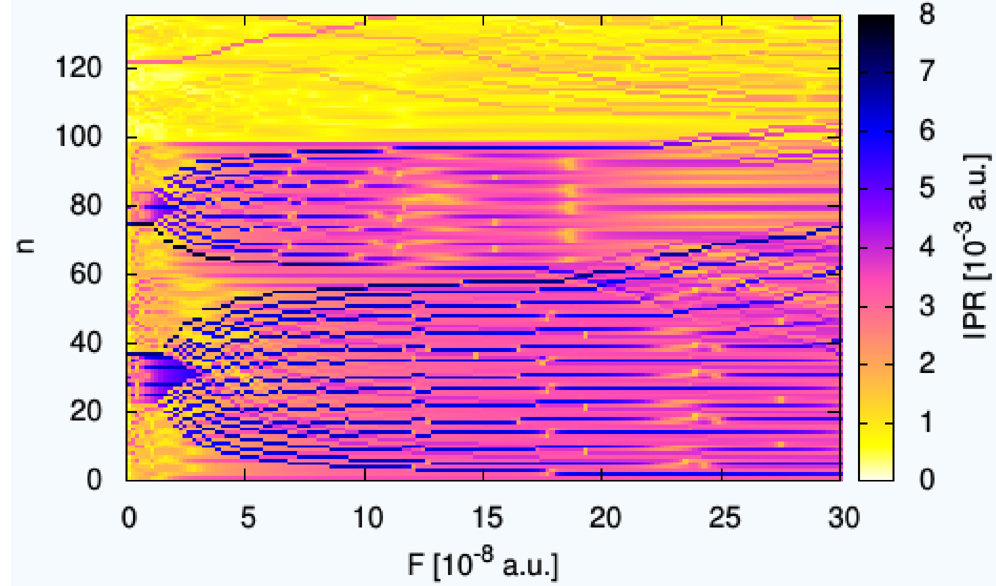

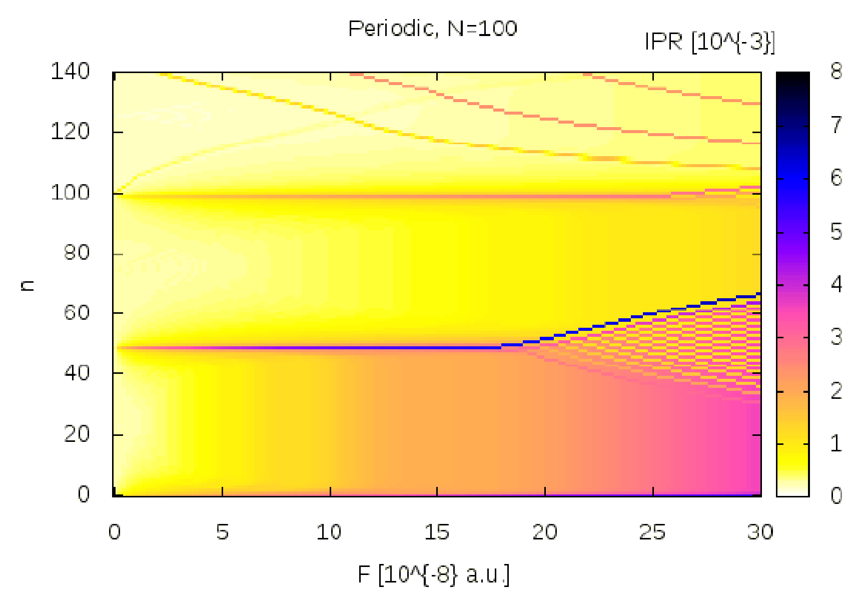

[Eur Phys J B **85**, 10 (2012)]

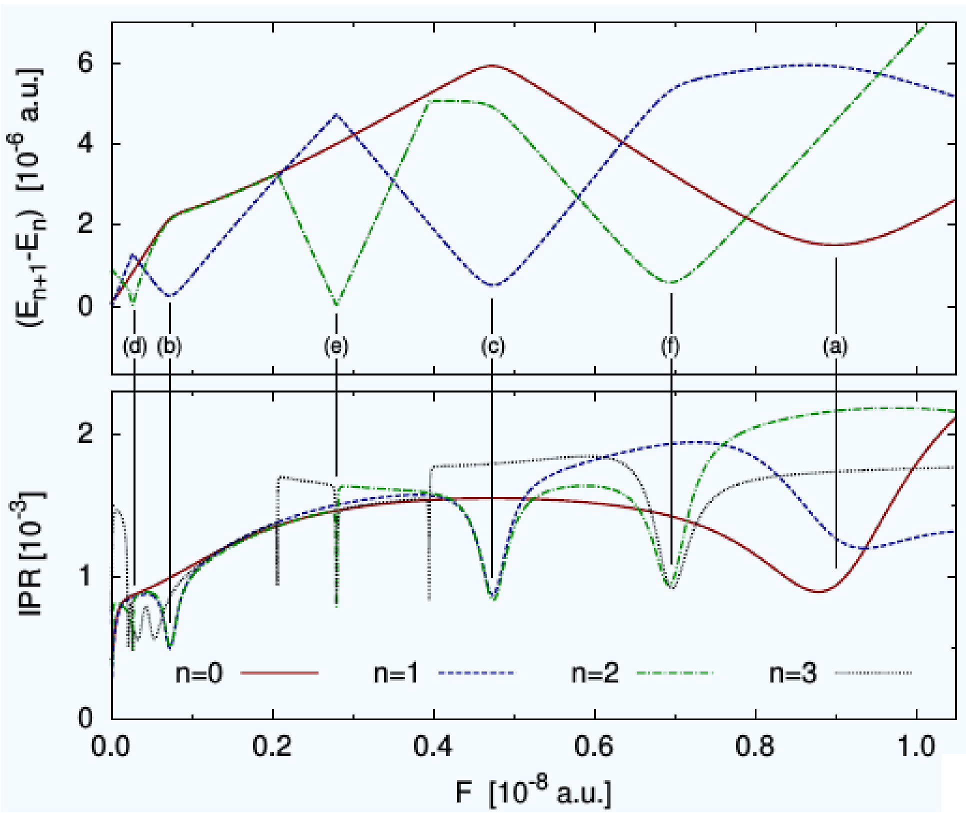

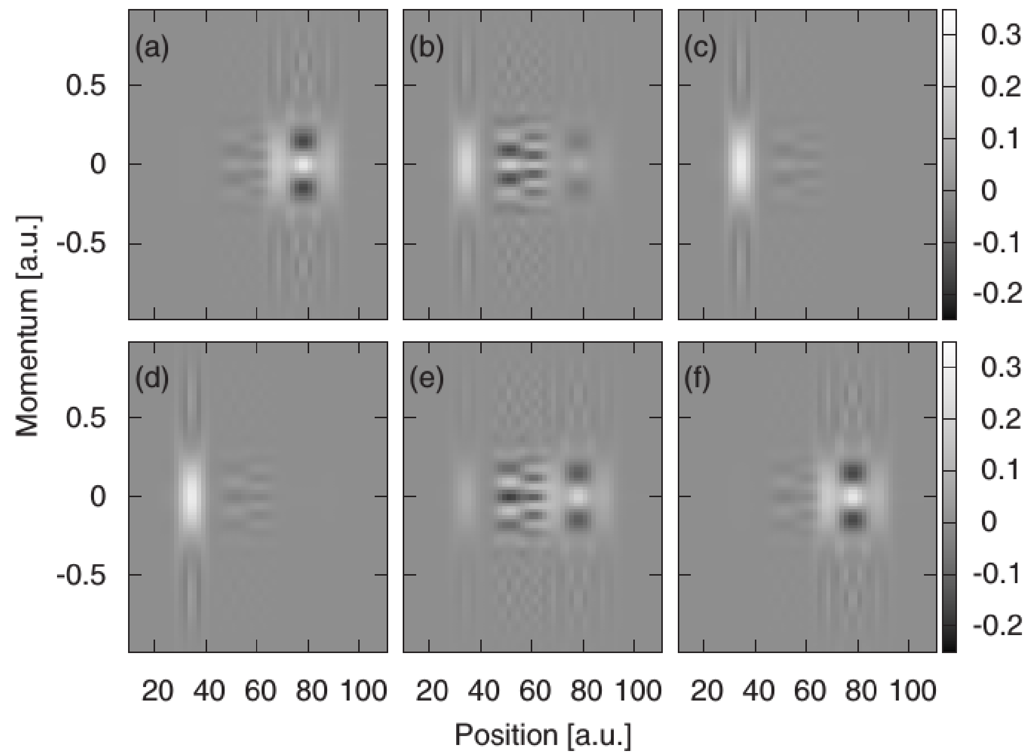

FIG. 3. The Wigner function for the system based on the Fibonacci sequence. (a)–(c) $n=0$ and (d)–(f) $n=1$. Electric field, from

[Phys Rev B **80**, 035127 (2009)]

- spektrum multifraktalne *f(α)*

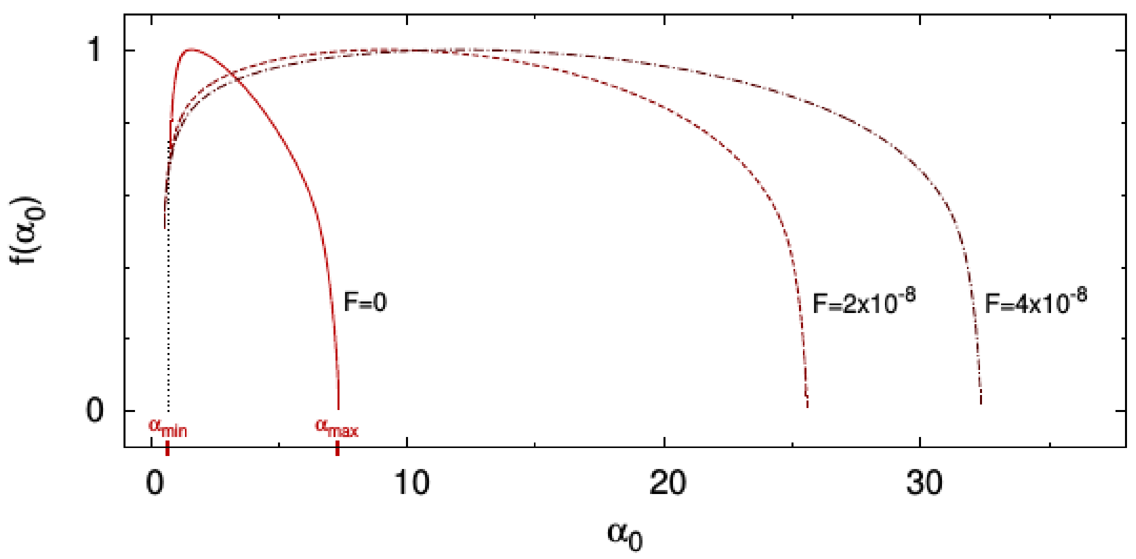

$$f\left(\alpha_n\right) = \lim_{\delta\to 0} \frac{\sum_{k=1}^{N(\varepsilon)} \mu_{nk}(\varepsilon;q)\ln\mu_{nk}(\varepsilon;q)}{\ln\delta}$$

$$\alpha_n(q) = \lim_{\delta\to 0} \frac{\sum_{k=1}^{N(\varepsilon)} \mu_{nk}(\varepsilon;q)\ln\mu_{nk}(\varepsilon;1)}{\ln\delta}$$

$$\delta = \varepsilon/L$$

$$\mu_{nk}(\varepsilon;q) = \frac{P_{nk}^q(\varepsilon)}{\sum_{j=1}^{N(\varepsilon)} P_{nj}^q(\varepsilon)},$$

$$P_{nk}(\varepsilon) = \int_{B_k(\varepsilon)} dx\,\left|\psi_n(x)\right|^2$$

$$D_n(q) = \frac{f\left(\alpha_n\right) - q\alpha_n(q)}{1-q}$$

- wymiar uogólniony *D(q)*

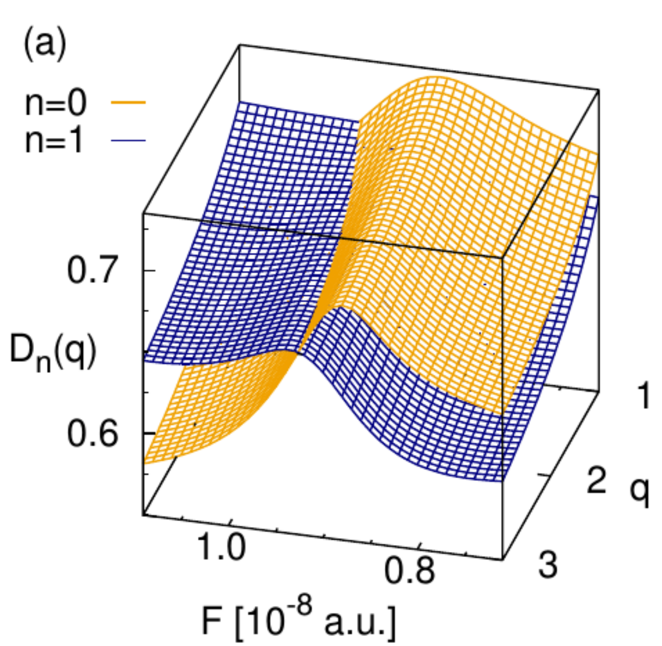

Nanodruty w zewnętrznym polu magnetycznym

- hamiltonian uwzględniający pola elektryczne ***F****=(0,0,F)* oraz magnetyczne ***B****=(0,0,B)*

$$\hat{\mathcal{H}} = \frac{1}{2m^*}[\hat{\mathbf{p}} + e\mathbf{A}(\mathbf{r})]^2 + U_{\mathrm{conf}}(\mathbf{r}) + eFz$$

$$U_{\mathrm{conf}}(x, y, z) = U_{\perp}(x, y; z) + U_{\parallel}(z) \qquad \psi(x, y, z) = \sum_s \phi_s(z)\chi_s(x, y; z)$$

- cechowanie symetryczne ***A*** *=* *(* ***B*** *x* ***r*** *) / 2*

$$\chi_s(x, y; z) = \sum_{k=1}^{N_x}\sum_{l=1}^{N_y} c_{kl}^s(z) g_{kl}(x, y; z)$$

$$g_{kl}(x, y; z) = \exp\left[-\frac{(x - x_k)^2 + (y - y_l)^2}{2\sigma^2} + \mathrm{i}\frac{(xy_l - yx_k)}{2\ell_B^2}\right]$$

$$c_{kl}^s(z)$$

$$E_s^{\perp}(B; z)$$

$$\left[-\frac{\hbar^2}{2m^*}\frac{\mathrm{d}^2}{\mathrm{d}z^2} + E_s^{\perp}(B; z) + eFz - (E - E_c)\right]\phi_s(z) = \sum_{s'}\left[\hat{T}_{ss'}(z) + \hat{A}_{ss'}(z)\right]\phi_{s'}(z)\,,$$

$$\left\{\begin{array}{l} \hat{T}_{ss'}(z) = \int \mathrm{d}x\mathrm{d}y\, \chi_s^*(x, y; z)\dfrac{\hat{p}_z^2}{2m^*}\chi_{s'}(x, y; z), \\ \\ \hat{A}_{ss'}(z) = \int \mathrm{d}x\mathrm{d}y\, \chi_s^*(x, y; z)\dfrac{\hat{p}_z}{m^*}\chi_{s'}(x, y; z)\hat{p}_z\,. \end{array}\right.$$

Nanodrut InAs z przewężeniem – magnetoopór

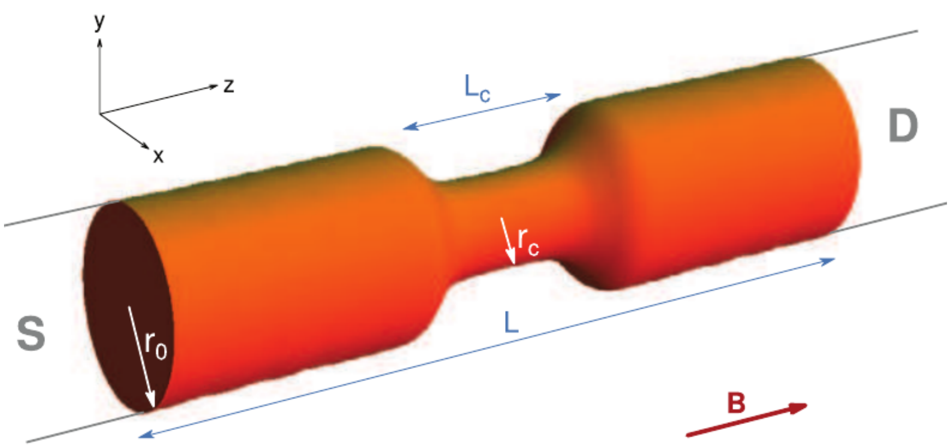

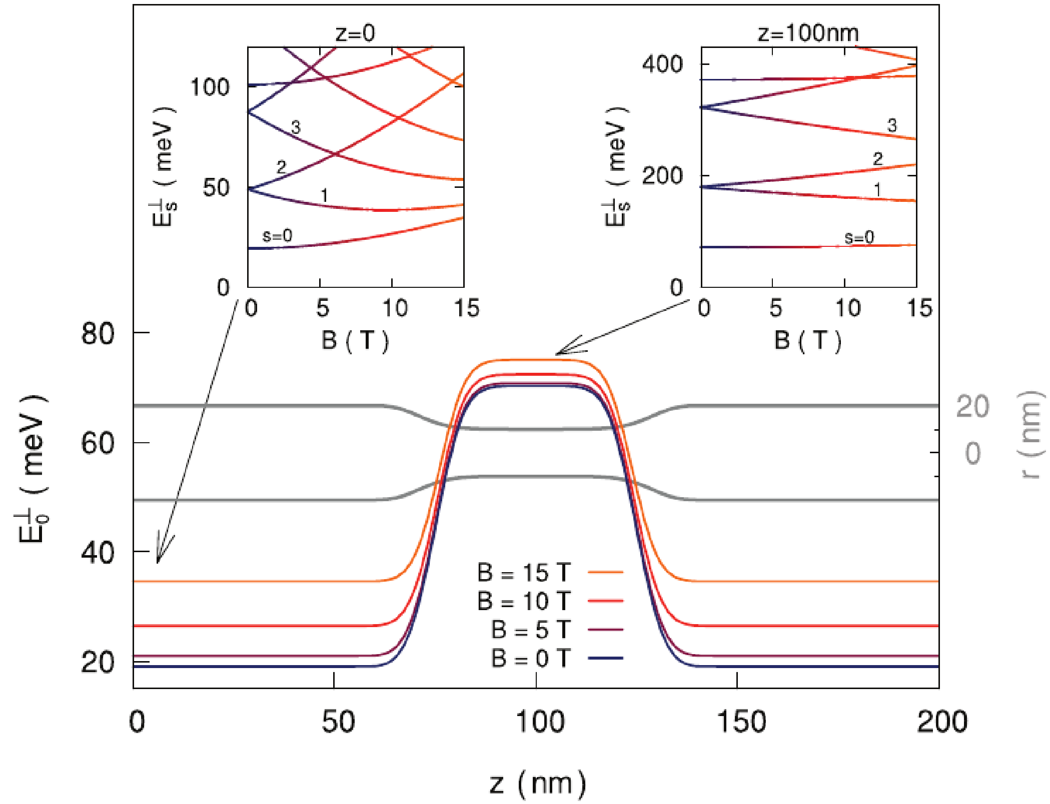

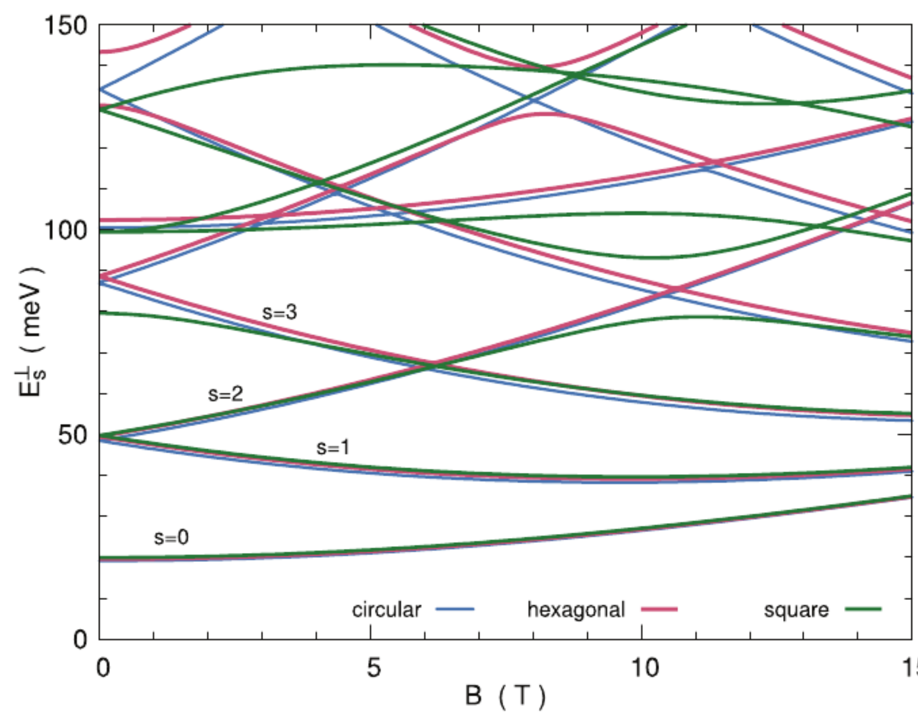

$$r(z) = r_0 - (r_0 - r_c)\,\exp\left[-\left|\frac{z-z_0}{L_c/2}\right|^p\right]$$

$L = 200nm$
$r_0 = 20nm$

$L_c = 60nm$
$r_c = 10nm \qquad p = 6$

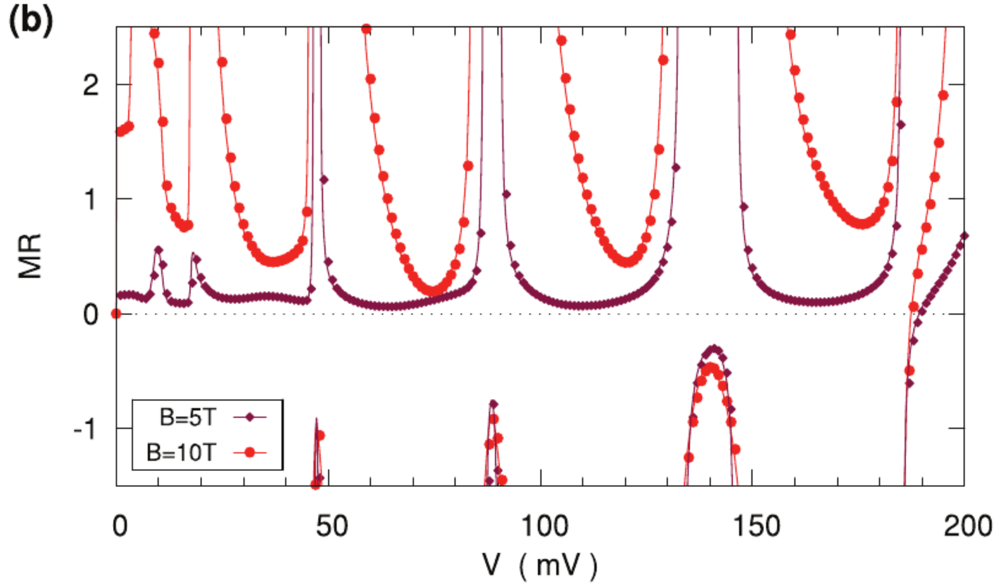

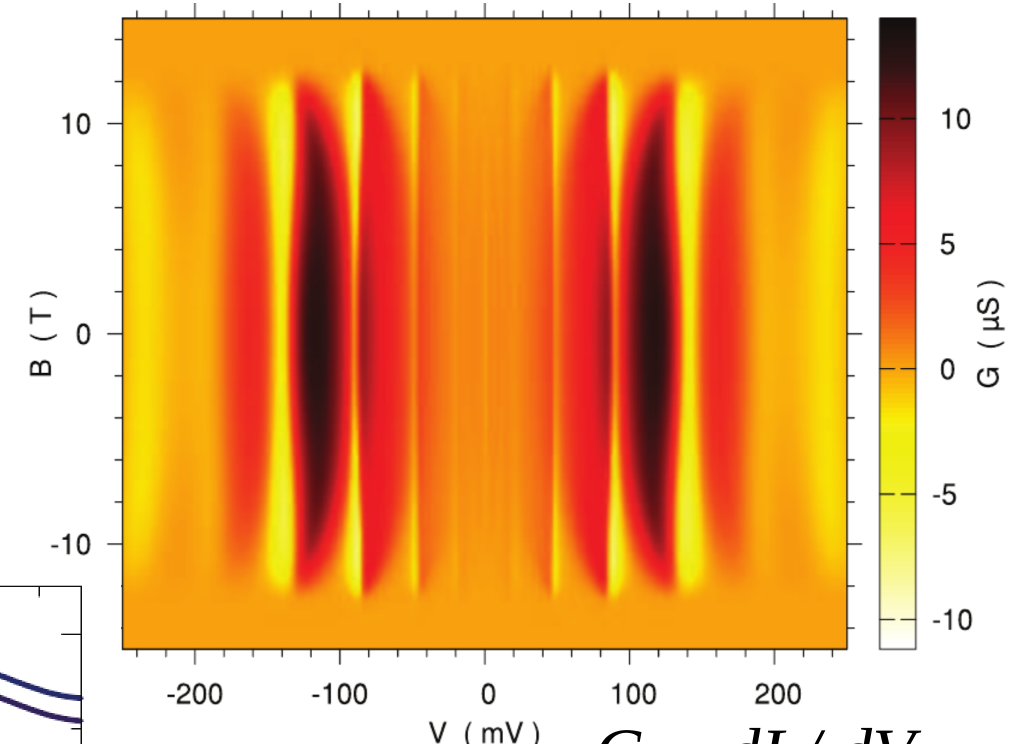

$$G = dI / dV$$

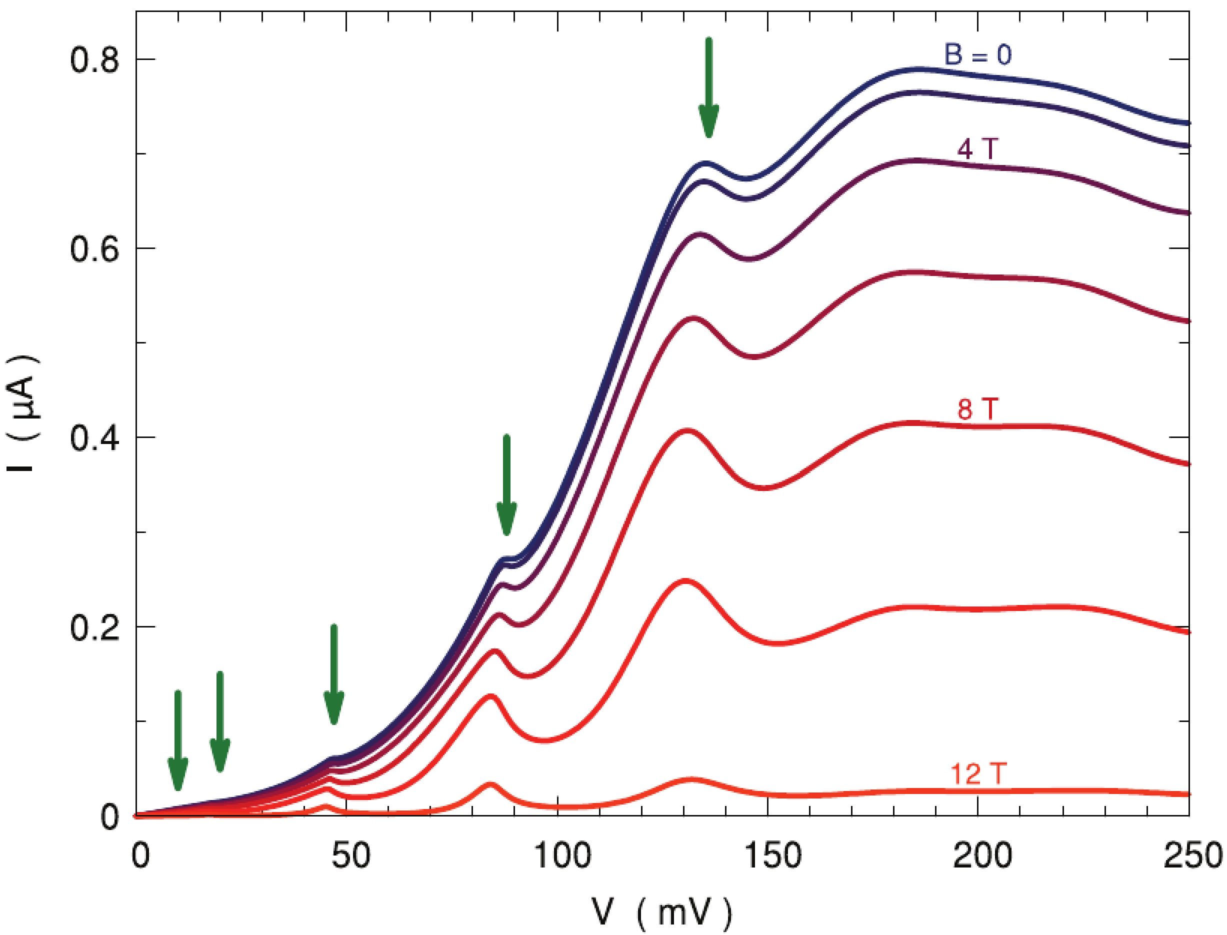

[J Phys Cond Mat **26**, 325301 (2014)]

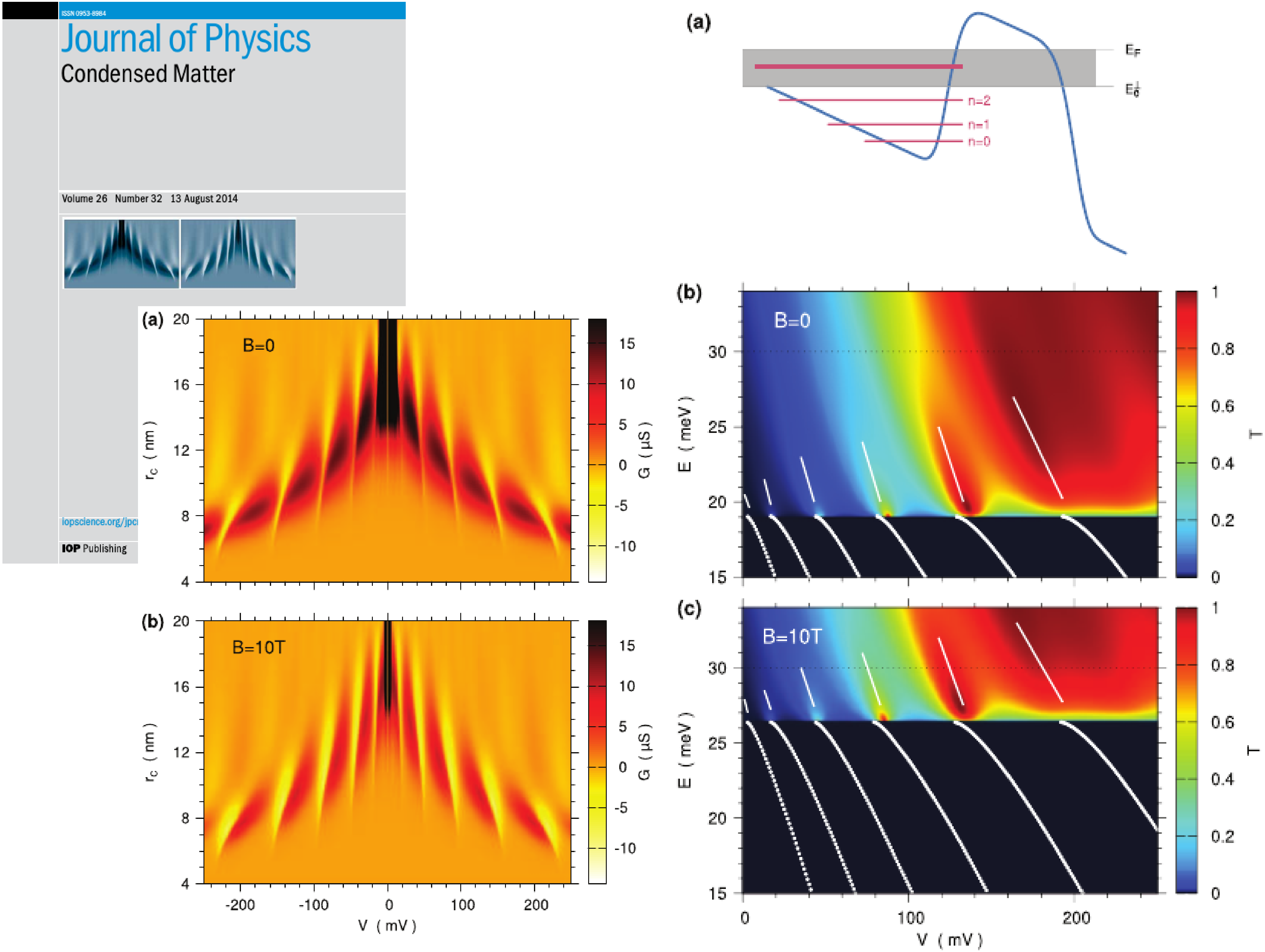

ISSN 0953-8984
Journal of Physics
Condensed Matter
Volume 26 Number 32 13 August 2014
iopscience.org/jpc
IOP Publishing
(a)
B=0
r_c (nm)
G (μS)
(b)
B=10T
V (mV)
(a)
E_F
E_0^i
n=2
n=1
n=0
(b)
B=0
E (meV)
T
(c)
B=10T
V (mV)

Transport zależny od spinu elektronu w nanodrucie InSb

$$\begin{bmatrix} \hat{\mathcal{H}}_0 + g^*\mu_B B - E & 0 \\ 0 & \hat{\mathcal{H}}_0 - g^*\mu_B B - E \end{bmatrix} \begin{bmatrix} \psi_\uparrow(\mathbf{r}) \\ \psi_\downarrow(\mathbf{r}) \end{bmatrix} = \begin{bmatrix} 0 \\ 0 \end{bmatrix}$$

$$g^*(B;\,z) = g\left[1 + \left(1 - \frac{m_0}{m^*}\right)\frac{\Delta_{SO}}{3[E_g + E_0^{\perp}(B;\,z)] + 2\Delta_{SO}}\right]$$

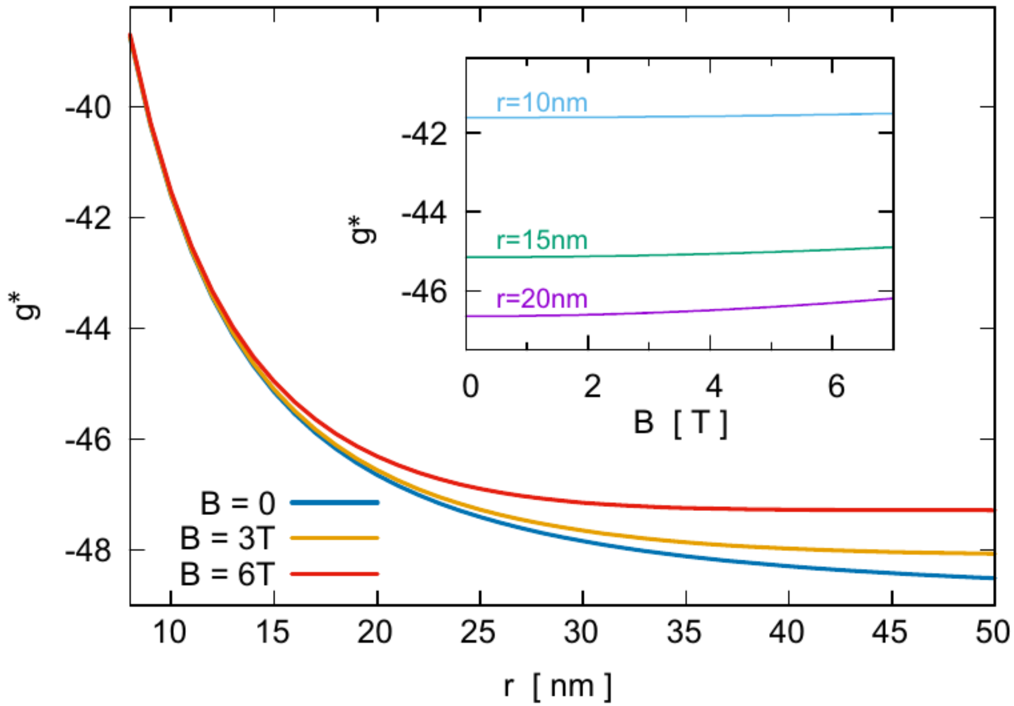

Fig. 2. Effective Landé factor g^* as a function of the nanowire radius r. in the presence of the magnetic field $B=0$ T, 3 T, and 6 T. Insets show g^* as a function of the magnetic field B calculated for the nanowire with radius r equal to 10 nm, 15 nm, and 20 nm.

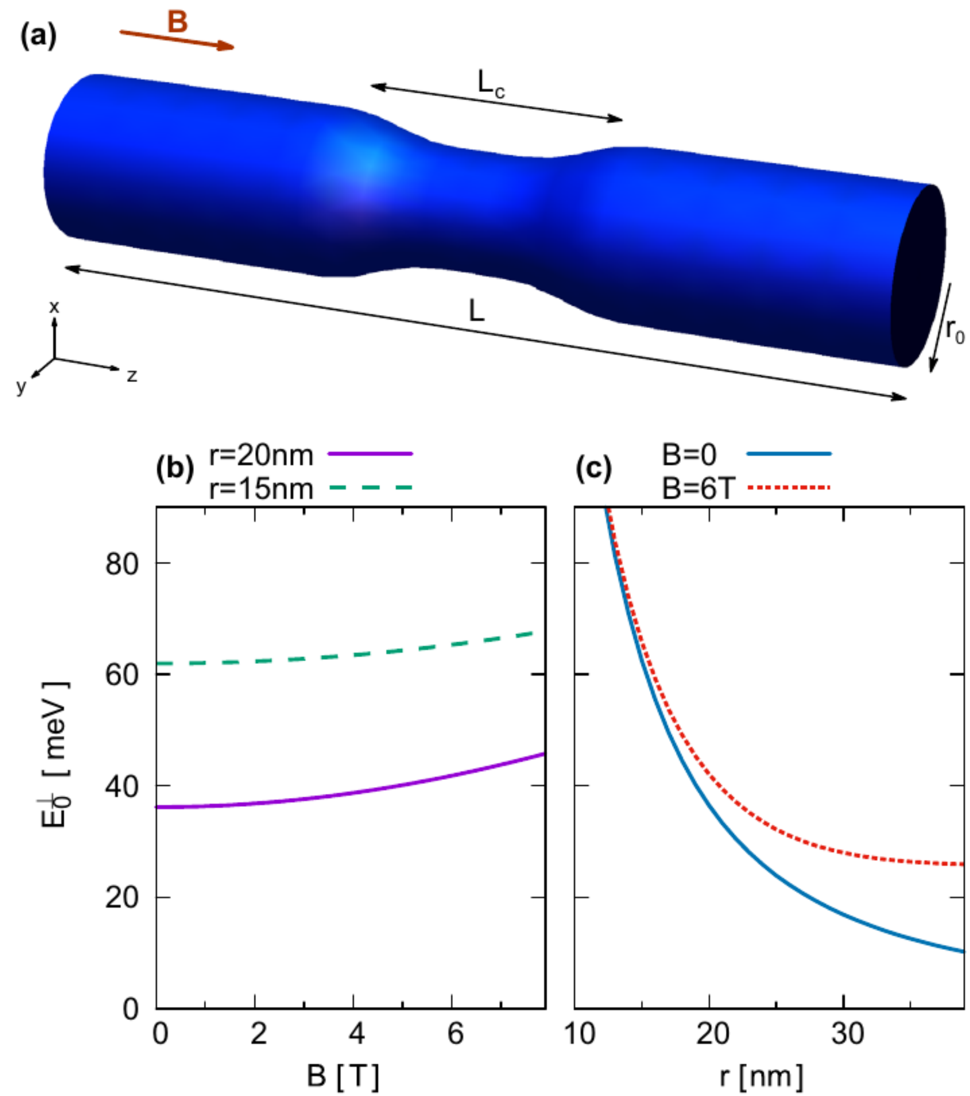

[Physica E **83**, 127 (2016)]

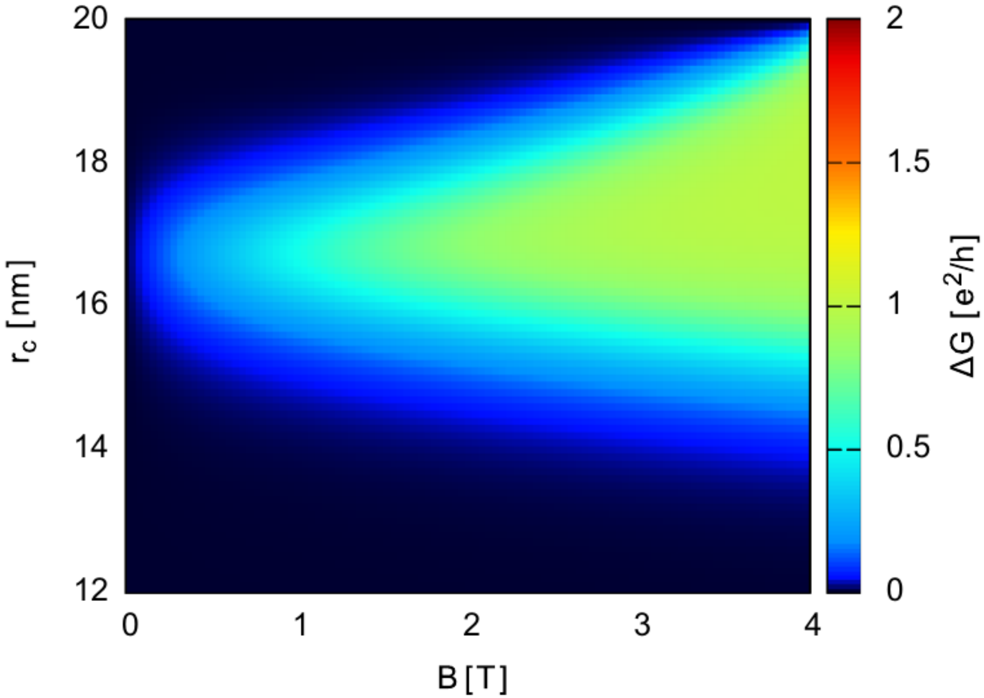

Fig. 3. Spin conductance ΔG as a function of the constriction radius r_c and the magnetic field B for the Fermi energy $E_F = 50$ meV.

$$\Delta G(B) = G_{\uparrow}(B) - G_{\downarrow}(B).$$

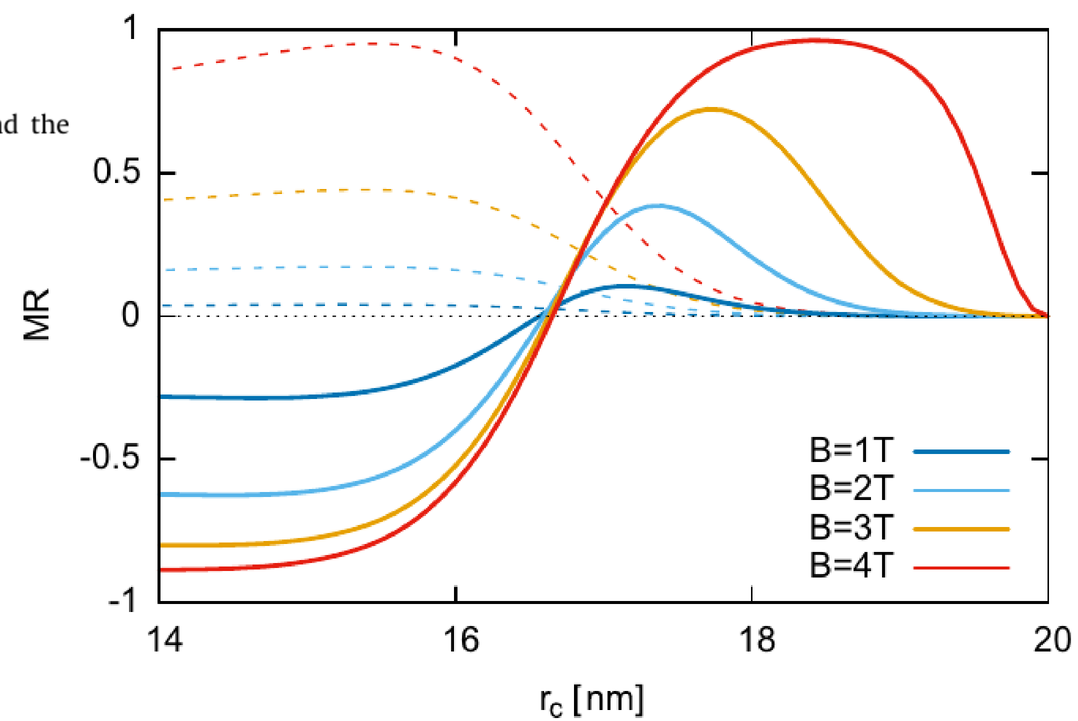

Fig. 4. Magnetoresistance as a function of: (a) radius r_c of the constriction and magnetic field B and (b) radius r_c of the constriction (cross sections of (a) at different B; dashed lines correspond to the results obtained when spin of the electrons is neglected).

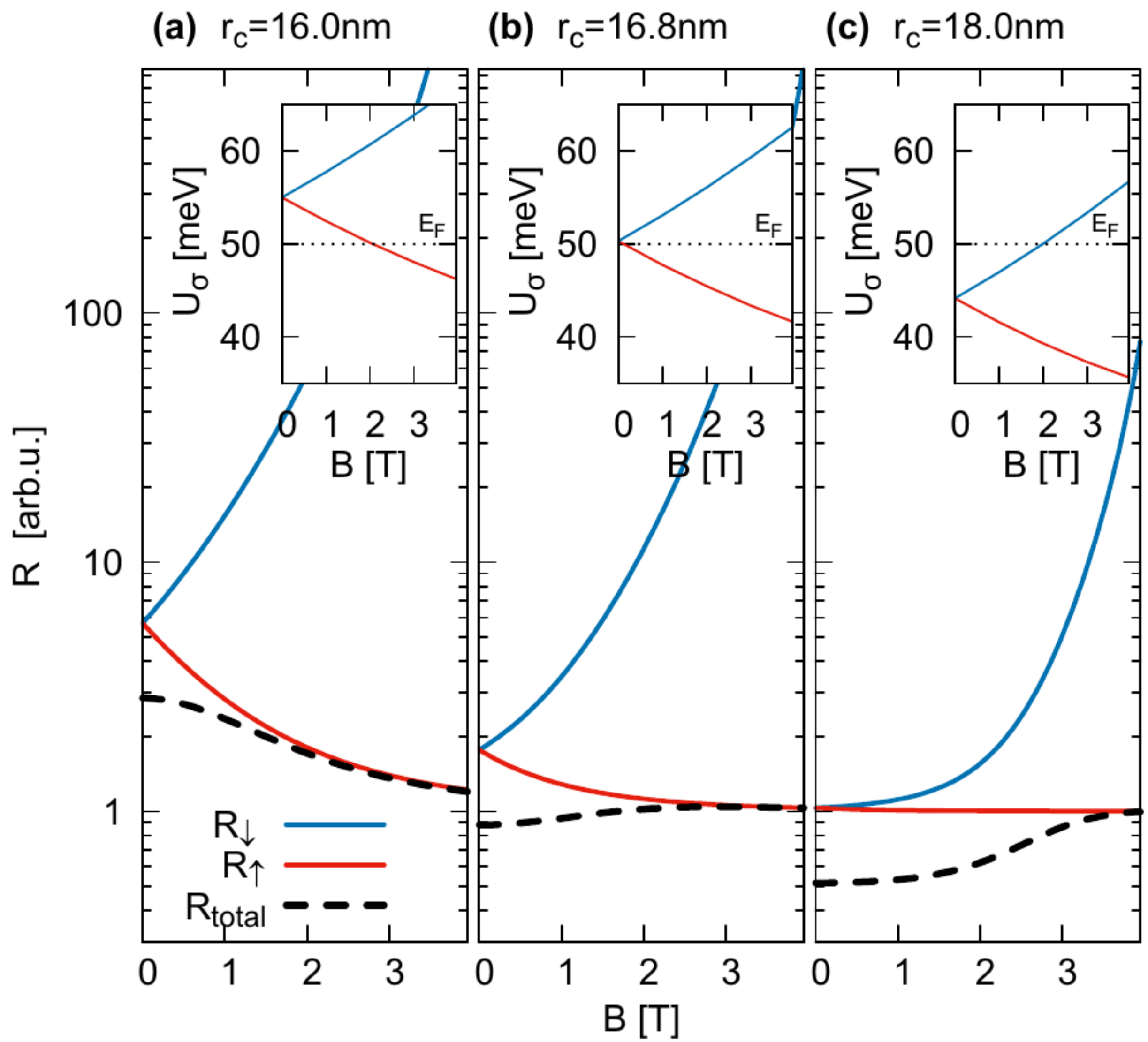

Fig. 5. Spin-up ($R_\uparrow$, red curves), spin-down ($R_\downarrow$, blue curves) and total (R_{total}, dashed lines) resistances of the nanowires for three different constriction radii r_c: (a) 16 nm, (b) 16.8 nm, and (c) 18 nm. Insets show the effective heights of barriers at the centers of constrictions, i.e., $U_\sigma = E_0^\perp(B; z_0) \pm g^*(B; z_0)\mu_B B$, and E_F is the Fermi energy. (For interpretation of the references to color in this figure caption, the reader is referred to the web version of this paper.)

Nanodrut InAs

3 bramki typu *all-around* → 2 sprzężone kropki kwantowe

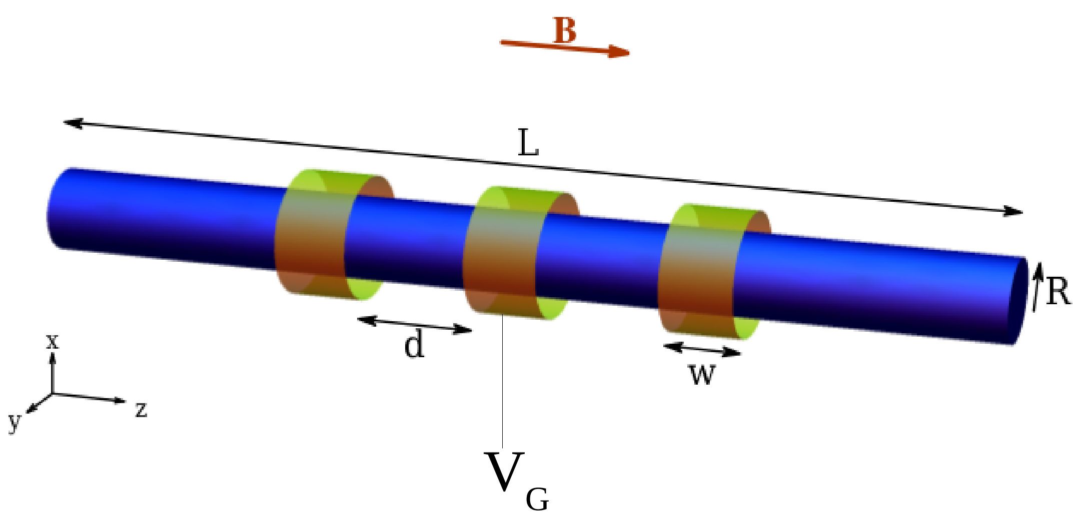

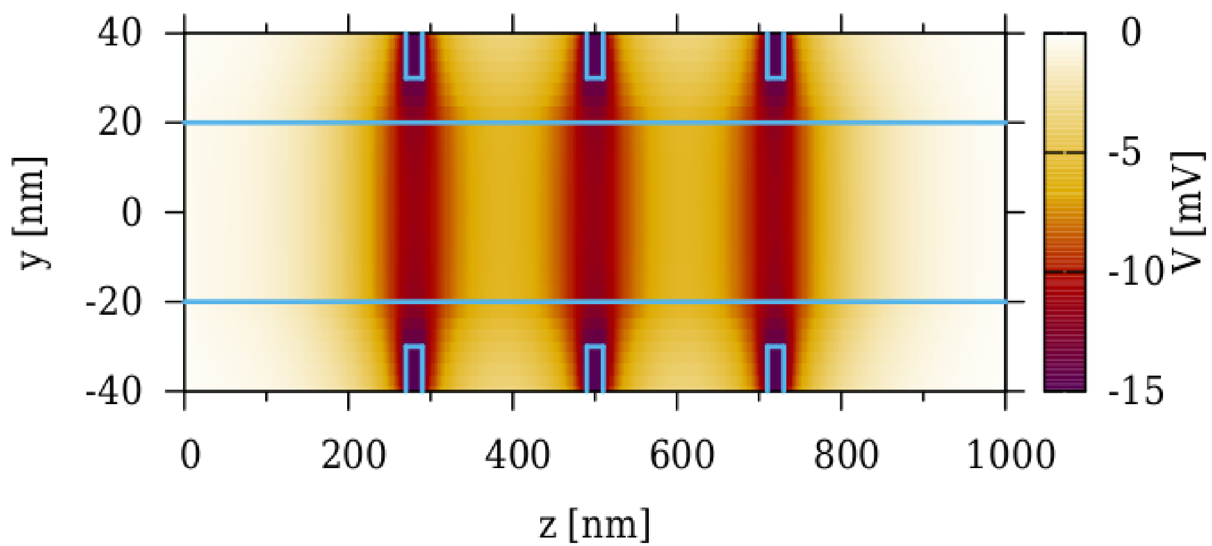

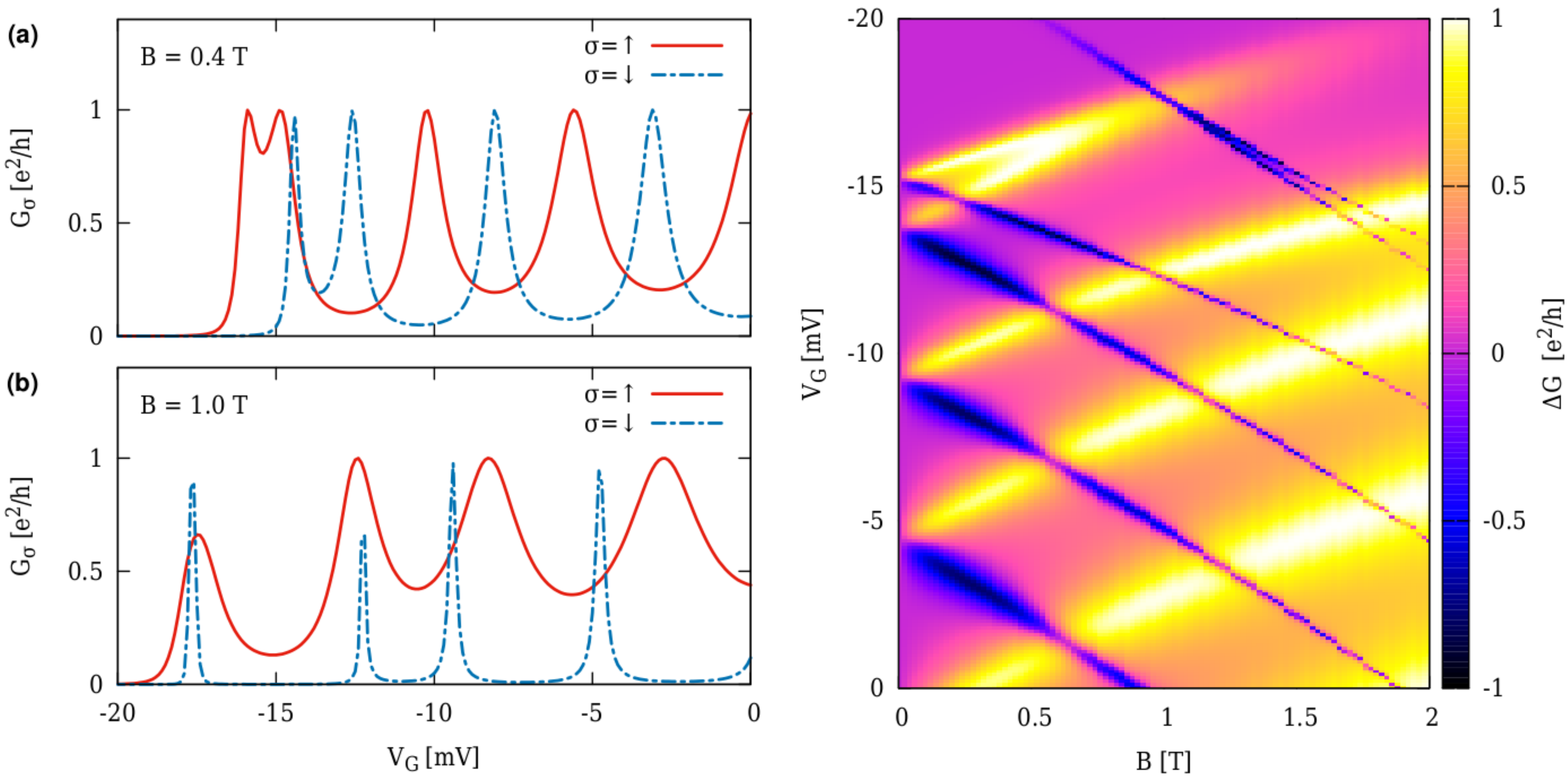

(a)
B = 0.4 T
σ=↑
σ=↓
G_σ [e^2/h]
(b)
B = 1.0 T
σ=↑
σ=↓
G_σ [e^2/h]
V_G [mV]
V_G [mV]
B [T]
ΔG [e^2/h]

5 bramek typu *all-around*

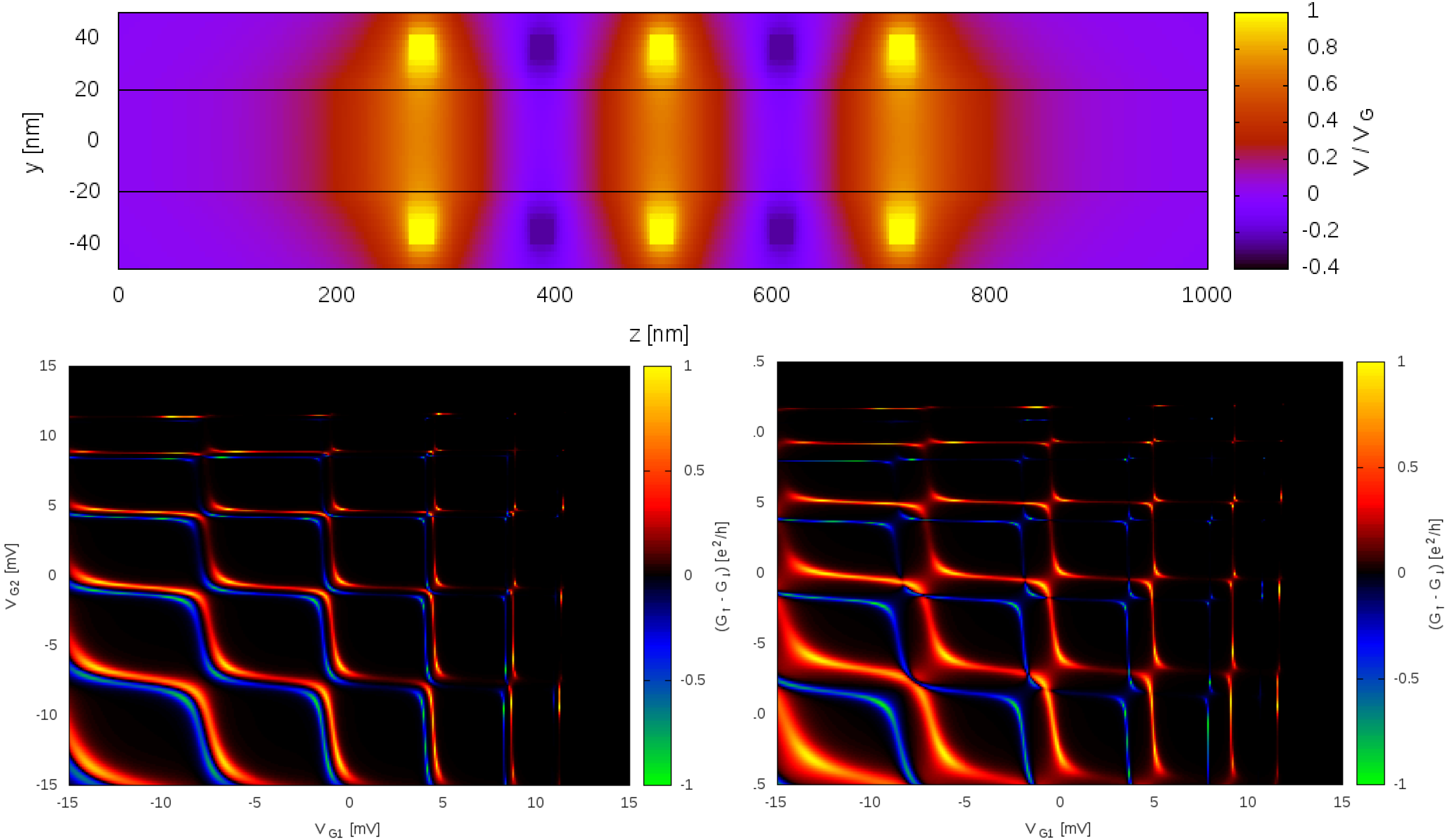

Podsumowanie

- oscylacje prądowe w nanodrutach tunelowo-rezonansowych
- transport elektronów w układach kwaziperiodycznych
- magnetoopór w drutach ze zmienną średnicą
- prądy zależne od spinu

Dziękuję za uwagę!